ANL-78-41

COMPARISONS OF SODIUM VOID AND DOPPLER REACTIVITIES IN LARGE OXIDE AND CARBIDE LMFBRs

by

S. F. Su

BASE TECHNOLOGY

U of C-AUA-USDOE

ARGONNE NATIONAL LABORATORY, ARGONNE, ILLINOIS

Prepared for the U. S. DEPARTMENT OF ENERGY
under Contract W-31-109-Eng-38

Printed in the United States of America
Available from
National Technical Information Service
U. S. Department of Commerce
5285 Port Royal Road
Springfield, Virginia 22161
Price: Printed Copy $5.25; Microfiche $3.00

Distribution Category:
LMFBR Physics (UC-79d)

ANL-78-41

ARGONNE NATIONAL LABORATORY
9700 South Cass Avenue
Argonne, Illinois 60439

COMPARISONS OF SODIUM VOID AND DOPPLER REACTIVITIES IN LARGE OXIDE AND CARBIDE LMFBRs

by

S. F. Su

Applied Physics Division

March 1978

TABLE OF CONTENTS

LIST OF FIGURES

LIST OF FIGURES (Contd.)

LIST OF TABLES

LIST OF TABLES (Contd.)

COMPARISONS OF SODIUM VOID AND DOPPLER REACTIVITIES IN LARGE OXIDE AND CARBIDE LMFBRs

by

S. F. Su

ABSTRACT

Sodium void and Doppler reactivities in two full scale (3000 MWth) LMFBRs are analyzed; one is fueled with UO_2 - PuO_2 and the other is fueled with UC - PuC. These two reactors are analyzed for beginning of life as well as for beginning and end of equilibrium cycle conditions, and the variations of these two safety parameters with burnup are explained. A series of comperative analyses of these two and several hypothetical reactors are carried out to determine how differences in fuel type, sodium content, and heavy metal concentration between an oxide and a carbide reactor affect their sodium void and Doppler reactivities. The effect of the presence of control poison on sodium void reactivity is also addressed.

I. INTRODUCTION

A. Scope of Work

This report presents a detailed discussion of the sodium void reactivities and Doppler coefficients of two full scale (3000 MWth) LMFBRs; one is fueled with UO_2-PuO_2, and the other is fueled with UC-PuC. These two reactors were analyzed for beginning of life (BOL) conditions as well as for beginning and end of equilibrium cycle conditions (BOEC, EOEC), so that the effects of burnup on these safety parameters can be seen. Reasons for the differences in safety parameters between carbide and oxide fueled LMFBRs were identified through a series of comparative analyses.

Section II describes the methods used in calculations of the sodium void reactivities and Doppler coefficients. Section III describes the designs and characteristics of the two reactors. The results of the sodium void reactivities and Doppler coefficients are given in Sections IV and V, along with the comparisons between the two reactors. Conclusions of the study are presented in Section VI.

B. Background

Sodium Void Reactivity

The reactivity change resulting from sodium voiding in a liquid metal fast breeder reactor (LMFBR) arises from changes in neutron leakage, spectrum and capture. It can be positive or negative for the reactor as a whole. The leakage component of the sodium void reactivity, resulting from change in the reactor transport cross section due to removal of sodium, has always a negative reactivity effect, and its contribution is greater the smaller the reactor is. The spectral component, originating from change in the elastic and inelastic scattering cross sections, is positive. This component becomes increasingly positive as fissile material concentration decreases.[1] It is more important for ^{239}Pu fuel than for ^{235}U fuel because η for ^{239}Pu increases more rapidly with energy than η for ^{235}U does. The third component of the sodium void effect comes from the change in the reactor macroscopic capture cross section. This component is positive, but its contribution is usually much less than the spectral component. In early fast reactor designs the cores were small and high concentration ^{235}U fuel was used. For these cores the negative leakage component dominated over the others. Later, as interest shifted to larger reactors needing a lower concentration of ^{239}Pu fuel, the positive components became more dominant and the reactor sodium void reactivity became positive.

While the terms "positive" and "negative" sodium void reactivity are usually used to describe the effect on reactor eigenvalue due to the removal of sodium from the reactor, it is important to note (a) the reactor sodium void reactivity is an integral data. The center region of the reactor usually shows a positive sodium void reactivity contribution, whereas in the outer core region the enhanced neutron leakage is responsible for a negative reactivity contribution. (b) An overall negative sodium void reactivity for a reactor does not exclude regions in the reactor which could have several

dollars worth of positive sodium void reactivity. (c) Whenever sodium void reactivity values are quoted, one has to know what regions have been voided (core, axial and radial blankets, control rod channels).

Doppler Reactivity

The reactivity effect resulting from fuel heating arises from changes in fission and capture resonances. Broadening of fission resonances has a positive reactivity effect and broadening of capture resonances has a negative reactivity effect. Changes in fission and capture resonances also affect the leakage process. However, the (positive) reactivity effect of this process is less significant unless the reactor is extremely small. The net reactivity change due to change in fuel temperature is more negative the larger the fertile-to-fissile ratio is. As a consequence, the Doppler effect is more negative for larger reactors with lower fissile material concentrations than for small reactors requiring higher fissile enrichments. The fertile-to-fissile ratio also affects the Doppler effect in another respect. Since cross section variations with temperature are more markedly at low energies, a higher fertile-to-fissile ratio, and consequently a softer neutron spectrum, tend to make the temperature reactivity effect of a large reactor increasingly more negative.

II. METHODS OF CALCULATIONS

The sodium void reactivity and the Doppler coefficient were calculated using the two-dimensional diffusion-theory capabilities of the ARC system.[2] Direct eigenvalue calculations were employed to determine reactivity changes. In some instances the first-order perturbation approximation was also used for purposes of comparison (see the Appendix). The first-order perturbation approximation was also used in obtaining detailed spatial distribution of sodium void reactivity. In all cases, calculations were carried out in R-Z models of the reactors using 21 energy groups.

The equilibrium cycle compositions of the reactors were calculated using the REBUS-2 fuel cycle code.[3] The flux iteration and control rod search to maintain criticality were included in the fuel cycle calculations. To take into consideration non-uniform burnup, the core and blankets of the reactors were subdivided into several burn regions. Eight energy groups were used in the fuel cycle calculations.

All the broad-group cross section sets used in this study were based on ENDF/B version IV data with the exception of the cross sections of three lumped fission products, which were based on ENDF/B version III data. Two 212-group cross section sets, which excluded fission and capture resonances, were first generated for each reactor using MC^2-2.[4] One set corresponded to a voided reactor composition and the other to a non-voided composition. These fine-group cross section sets were then used to generate broad-group cross sections for appropriate temperatures using the SDX code,[5] through which self-shielded resonance cross sections were calculated by treating individual reactor regions heterogeneously.

The sodium void reactivity was calculated for voiding of the inner core, voiding of the outer core, voiding of the whole core, and voiding of the entire reactor. In calculating the sodium void reactivity of a particular region, the broad-group cross sections generated for the voided composition were used in that region and the cross sections generated for the unvoided composition were used elsewhere. In calculations of the total Doppler coefficient of a reactor the fuel temperature and its change were assumed uniform throughout the reactor (isothermal Doppler). The Doppler contributions of individual regions were calculated in a sequential manner in which the fuel temperatures of the inner core, outer core, axial blanket and radial blanket were varied one by one and in that order. The fuel temperature of each region remained uniform within itself. Temperatures used in calculations of the Doppler coefficient were 650, 1300, and 2200°K for the oxide reactor and 650, 1100, and 2200°K for the carbide reactor (the Doppler broadening of resonances are treated for all isotopes with a mass number of greater than 100). 1300°K for the oxide reactor and 1100°K for the carbide reactor were the assumed fuel temperature under normal operation. These were the temperatures at which the sodium void reactivities were calculated.

III. REACTOR DESIGNS AND PERFORMANCES

A. 3000 MWth Oxide Reactor

The planar layout of the 3000 MWth oxide reactor is shown in Fig. 1. The core has two enrichment zones. The inner core occupies ten rows and the outer core covers three rows. There are nineteen control rod positions in the entire core. The outer core is surrounded by three rows of radial blanket followed by one row of radial reflector.

The core is 40 inches high, and the axial blanket and reflector are 13 and 3 inches thick, respectively. The fuel pin is 0.300 inches in diameter with a pitch-to-diameter ratio of 1.208. The volume fractions of fuel, structure (SS316 CW), and coolant in the core are 0.3845, 0.2157, and 0.3848, respectively. In the radial blankets these fractions are 0.5975, 0.1613 and 0.2412, respectively. The smeared fuel densities are 88, 91.4 and 95% T.D., respectively, in the core, the axial blanket, and the radial blanket. The maximum pellet discharge burnup of the core is 71,300 MWD/MT.

The reactor is designed for a cycle length of one year with a 82.2% load factor, i.e., 300 full power days (FPD) per year. The fuel residence time is taken to be two years for the core (and the axial blanket) and five years for the radial blanket. Light water reactor discharged plutonium is used as fuel. Detailed design information is delineated in Table I.

The performance characteristics of the reactor at the beginning of life and the beginning and end of equilibrium cycle are summarized in Table II. The reactor loses reactivity with burnup with a reactivity swing of Δk_{eff} = -0.0221 over the equilibrium cycle. The charge fuel enrichments of the inner and outer cores at BOL and at BOEC produce an excess reactivity of that amount. The 7th and 11th-row control rods are inserted and gradually removed to maintain criticality during fuel cycle calculations using REBUS-2. These two rows of control rods are chosen because they are closer to the outer core, in which the power swing is much greater than in the inner core due to a relatively low fissile conversion ratio there.

The reactor breeding ratio is 1.29 at BOL, 1.26 at BOEC, and 1.25 at EOEC. The equilibrium compound system doubling time of 25.6 years is based on an external cycle length of one year and a 2% fissile material reprocessing and fabrication loss. Such a compound system doubling time, due to conservative nature of the design, is somewhat longer than for later designs.[6] However, it has been verified that the sodium void reactivity and the Doppler coefficient of this reactor are very close to those of a geometrically similar, but more optimistically designed reactor, which has a compound system doubling time of 17.6 years (the differences in these two reactivity coefficients between the two designs are no greater than 4%). The specific inventories listed in Table II are based on a thermal efficiency of 40%.

The radial variations of the flux and power density at the mid-plane are plotted in Figs. 2 and 3. The locations of control rods are shown in these figures.

B. 3000 MWth Carbide Reactor

Design descriptions of the 3000 MWth carbide reactor are given in Table III. Its hexagonal arrangement is shown in Fig. 4.

The core has a total of eleven rows, of which two are in the outer core. Like the oxide reactor, this reactor also has three rows of blanket and one row of reflector. The number of control rods is nineteen. The axial dimensions, i.e., the core height, the blanket and reflector thicknesses, and the plenum length are exactly the same as in the oxide reactor. However, the plenum is now at the top. The sodium-bonded fuel pins have a diameter of 0.375 inch, and the pitch-to-diameter ratio is 1.263. The volume fractions in the core are 0.3757 fuel, 0.1427 structure, and 0.4816 coolant (including the sodium bond). For the radial blanket the same volume fractions were used as in the oxide reactor. The core and the axial blanket both assume a smeared fuel density of 89.6% T.D. (95% T.D. pellet). The maximum pellet discharge burnup is 67,000 MWD/MT. The smeared fuel density in the radial blanket is 95% T.D., the same as in the radial blanket of the oxide reactor.

The performance characteristics of the carbide reactor are given in Table IV. The breeding ratio at BOL is 1.62. It decreases to 1.57 at BOEC then to 1.47 at EOEC. The equilibrium compound system doubling time is 9.7 years.

In contrast to the oxide reactor, the carbide reactor gains reactivity with burnup. The initial and equilibrium charge enrichments correspond to an unpoisoned k_{eff} of 1.0 at BOL and BOEC. Since the fissile conversion ratio of the inner core is greater than unity while that of the outer core is below but much closer to unity, the power swing in the inner core tends to be greater than in the outer core. For this reason the central and fifth-row control rods are used to adjust for criticality during fuel cycle calculations. The flux and power distributions of the reactor at different time stages are plotted in Figs. 5 and 6.

IV. SODIUM VOID REACTIVITIES

A. Oxide Reactor

The sodium void reactivities for the oxide reactor at different stages of life, based on direct eigenvalue calculations, are given in Table V. The sodium void reactivities of the inner core, the outer core, and the entire core do not include contribution from removal of sodium from the control rod channels. The sodium void reactivity of the entire core is calculated by voiding the inner and outer core zones simultaneously. However, the reactivity worth so obtained is very close to the sum of the worths of the two core zones calculated independently (less than 2% difference). The voiding of the core included the removal of sodium from inside the fuel assembly as well as from the space between the fuel assemblies. While in the development of an accident the sodium between assemblies will leave the core much later than the coolant inside the fuel assemblies, it is difficult to determine accurately the amount of sodium between the fuel assemblies. This space was provided in the design to accommodate the duct dilation due to irradiation swelling and creep. Therefore, only at BOL is this space fully available. As burnup progresses this sodium will be expelled to some extent and therefore, the interassembly gap occupies less than the 9.2% (oxide) or 8.5% (carbide) of the core volume. In other words, while at BOL the coolant inside the fuel assemblies represents 76% of the total sodium inventory in the oxide core (compared to 82% for the carbide core), at later stages of life this fraction will be higher. To see the significance of the sodium gap between assemblies in voiding patterns, Tables V and VII show also the sodium void reactivities when the voiding of the interassembly gaps is excluded. The admittedly cruel assumption here was that the interassembly gap space is the same at BOL, BOEC and EOEC. For all other presentation of sodium void reactivities it was assumed that voiding of the core meant removal of sodium from inside the fuel assembly as well as the interassembly gap.

The total core sodium worth is 0.0203 $\Delta k/k$ at BOL, the majority of which is from the inner core. The worth increases slightly to 0.0226 $\Delta k/k$ at BOEC, then to 0.0256 $\Delta k/k$ at EOEC. The sodium reactivity worth of the entire reactor is about 10 to 18% less than that of the core, reflecting a negative contribution from the blankets and reflectors.

The sodium void reactivity of all control rod channels is positive at BOL and BOEC, but negative at EOEC. As mentioned earlier, since this reactor loses reactivity with burnup, it starts a burn cycle with the control rods inserted. The control rods are gradually withdrawn and completely removed at the end of the cycle to compensate for the reactivity loss. With the absence of control poison at EOEC, the negative leakage component of the sodium void effect due to the removal of sodium from the control rod channels exceeds the positive spectral and capture components, leading to a negative net sodium void reactivity. At BOL or BOEC when there is control poison in the core, the hardening of spectrum due to voiding reduces the reactivity worth of the control rods as well, and the net sodium void reactivity becomes positive at these two points. (The presence of control poison affects the sodium void reactivity of not just the control rod channels. The sodium void reactivity of any region would be more positive if the control rods are inserted. The effect of control poison on the sodium void reactivity of the core will be discussed in more detail later.)

In all the cases listed in Table V, a fuel temperature of 1300°K and a sodium density of 0.84 gm/cm^3 (corresponding to a coolant temperature of 733°K) were assumed. Furthermore, sodium-out cross sections were used in regions without sodium and sodium-in cross sections were used elsewhere. In order to have some understanding of the cross section sensitivity on sodium void reactivity, the effects of using sodium-in cross sections in all reactor regions to calculate the sodium void reactivity were analyzed. The core sodium void reactivity so calculated was only 0.0153 $\Delta k/k$, about 25% less than using sodium-out cross sections in the core. Limiting the sodium voiding in the core to the coolant only leads to a less than 25% reduction in sodium void reactivity.

The sodium void reactivity in the core has also been calculated using the first order perturbation theory. Table VI shows the leakage and spectral components as well as the net sodium worth in the core from perturbation calculations. The spectral component here includes also the capture component, and the leakage component includes a D/D' modification factor (with D and D' being the unperturbed and perturbed diffusion coefficients) to reduce overestimation of the leakage component expected from the first order perturbation approximation. The positive spectral component dominates over the negative leakage component all the time. Furthermore its value increases with burnup. The reason for this increase is the buildup of fission products, whose absorption cross sections decrease sharply and more markedly even for a slight increase in neutron energy than other nuclides. The magnitude of the leakage component, on the other hand, decreases with burnup because of the flattening of the flux, especially in the axial direction. Both the decrease in the magnitude of the leakage component and the increase in the spectral component are responsible for the increase in the total sodium void reactivity, although the latter is a more important factor.

Compared to the direct eigenvalue calculations the first order perturbation calculations underpredicted the core sodium void reactivity by 8.4 to 8.6%. The first order perturbation theory is not expected to be very accurate for such large reactivity changes.

The values in parentheses in Table VI are also from first order perturbation calculations but without taking into account microscopic cross-section changes due to spectral hardening when the core is voided. In other words, in these calculations the microscopic cross section generated for the flooded reactor were used both before and after the perturbation was introduced. This simplified calculational approach leads to 13 to 14% reduction in the spectral component and 17 to 20% reduction in the net sodium void reactivity. The leakage component is affected only slightly.

Figures 7-9 show, based on the perturbation calculations with proper accounting of the microscopic cross-section changes, the radial variations of sodium void reactivity at three axial locations, 0, 30 and 49 cm from the core midplane (the core-axial blanket interface is 50.8 cm from the midplane). The reactivity worth is expressed in terms of $\Delta k/k^2$ per unit reactor volume. It can be transformed into $\Delta k/k^2$ per unit volume of sodium by dividing it by the sodium volume fraction, which is 0.3848 for the core, or it can be transformed into $\Delta k/k^2$ per gm of sodium by further dividing it by the sodium density, taken to be 0.84 gm/cm^3 here. The bulk of the core is in the domain of positive sodium worth. Only very close to the edges of the core where the leakage is high does the sodium worth become negative.

The integral sodium void reactivity, integrated from the core centerline to a radius R within the core, is presented in the Appendix where the results of direct eigenvalue calculations as well as perturbation calculations are given and compared. The values of the core maximum sodium void reactivity given in Table V are the values of the integral sodium void reactivity, based on direct eigenvalue calculations, for the radius beyond which the the integral sodium void reactivity begins to decline.

B. Carbide Reactor

For calculations of the sodium void reactivity of the carbide reactor, the fuel temperature is taken to be 1100°K. The results of direct eigenvalue calculations are given in Table VII. The total sodium void worth of the core (excluding control rods) is very close to the combined worth of two core zones, as in the case of the oxide reactor. The sodium void reactivities of each core zone as well as of the entire core all increase with burnup. The rate of increase is larger for the carbide than for the oxide reactor (the total core sodium void reactivity increases by 17% over the equilibrium cycle, compared to a 13% increase for the oxide reactor). The sodium void reactivity of the entire core at EOEC is 0.0334 $\Delta k/k$ which is 30% higher than the corresponding stage of the oxide reactor.

The sodium void reactivity of the entire reactor is about 5 to 10% less than that of the core. The maximum radially-integrated sodium void reactivity is about 5% higher than the whole core. The sodium void reactivity of the control rod channels is negative at BOL and BOEC when there is no control poison in the core, indicating that the negative leakage component exceeds the positive spectral and capture components at those two time points. However, since the control rods are inserted at EOEC to offset the positive reactivity swing, the sodium void reactivity of the control rod channels becomes positive, because, as mentioned earlier, the spectrum hardening due to voiding also leads to a reduction in the control rod worth. Limiting the sodium voiding in the core to the coolant only leads to a less than 20% reduction in sodium void reactivity.

The spectral and leakage components and the net sodium void reactivity of the core, based on first order perturbation calculations are listed in Table VIII (the values in parentheses exclude the effects of microscopic cross-section changes due to spectral hardening). It is seen that the increases in the net sodium void worth with burnup arise mainly from the increases in the spectral component. Furthermore, the primary source of differences in the sodium void reactivity for this reactor and the oxide reactor is in the spectral component.

The spatial variations of the net sodium void reactivity as well as the spectral and leakage components are illustrated in Figs. 10-12. Notice that there is no control poison in the reactor at BOL and BOEC. At EOEC the central and fifth row control rods are inserted.

C. Oxide Reactor vs. Carbide Reactor

It has been shown previously that the sodium void reactivity is larger for the carbide reactor than for the oxide reactor. It has also been pointed out that the principal source of the differences between these two reactors lies in the spectral aspect of the void effect. In order to gain insight into the physics of these phenomena some neutronic parameters of the two reactors and their changes associated with voiding of the core are listed in Table IX.

The first parameters is the median energy of the neutron flux in the core. Indicative of the hardness of the neutron spectrum, it is about 21 to 28 keV higher for the carbide reactor than for the oxide reactor. It decreases with burnup for the oxide reactor, but the reverse is true for the carbide reactor. The increases in the median energy due to voiding are about 19 and 31 keV for the oxide and carbide reactors, respectively, reflecting the difference in the extent of spectrum hardening.

The number of fission neutrons released per neutron absorbed in the heavy metal (the second parameter) is larger for the oxide reactor than for the carbide reactor, because the former has higher fuel enrichments. The increase in this parameter, when the core is voided, arises from an increase in the threshold fissions of fertile nuclides and a decrease in the capture-to-fission ratio (the α-value) of the heavy metal, as a result of spectrum hardening. The magnitude of increase in this neutron yield per absorption in the heavy metal depends on several factors. First, a greater spectrum shift naturally would lead to a larger increase in the threshold fissions and a larger decrease in the capture-to-fission ratio. Secondly, a higher fertile-to-fissile ratio tends to give rise to a larger increase in the threshold fissions. In addition, an originally harder spectrum would also result in a larger increase in the threshold fissions when the spectrum hardens. All these factors point to a larger increase in the number of neutrons released per absorption in the heavy metal for the carbide core than for the oxide core when they are voided. The change in the neutron yield of the heavy metal is the most important source of the positive spectral component of the sodium void effect.

The third neutronic parameter connected to sodium voiding is the number of neutrons absorbed in heavy metal per neutron absorbed in the core. Table IX shows that the change in this parameter resulting from removal of sodium increases significantly with burnup for both cores. This phenomenum, as pointed out earlier, is due to the increasing concentrations of fission products, and is the main reason why the sodium void reactivities of the two reactors increase with burnup.

The last parameter in Table IX is the number of fission neutrons released per neutron absorbed in the core. It is the η value of the core and is equal to the multiplication of the second and third parameter. Its change due to voiding again is larger for the carbide core than for the oxide core.

Table IX has shown various neutronic parameters and their change associated with sodium voiding. However, it has not been explained why such differences exist. In order to be able to identify the causes for the difference in sodium void reactivity between the two reactors, some basic differences in properties of oxide and carbide reactors have to be examined.

The oxide and carbide reactors studied differ in three areas:

(1) the carbide reactor has a higher coolant volume fraction,

(2) the carbide reactor has a higher heavy metal concentration, and

(3) the carbide reactor has one carbon atom whereas the oxide reactor has two oxygen atoms per heavy metal atom in their fuel.

Before getting into the discussions of the effects of these differences one by one by analyzing the sodium void reactivities of some hypothetical reactors, another factor that also affects the calculations of sodium void reactivity will be discussed first: the impact of control rod insertion on the sodium void reactivity.

(1) Effects of Control Poison

It has been mentioned before that the oxide reactor has a negative burnup swing and thus requires some excess reactivity to cover this reactivity loss. Consequently, the sodium void reactivities of this reactor were calculated assuming it has an excess reactivity equal to the burnup swing and assuming the control rods are properly adjusted so that the reactor is always critical. In other words, the sodium void reactivities at BOL and BOEC were calculated in the presence of the control poison, and those at EOEC in absence of the control poison, In case of the carbide reactor, since the burnup swing is positive, the control poison is assumed present at EOEC, but not at BOL or BOEC when the reactor is critical without control poison.

Based on the above assumptions, the total core sodium void reactivity of the oxide reactor increases by 0.0030 $\Delta k/k$, from 0.0226 to 0.0256 $\Delta k/k$, over the equilibrium cycle, compared to a 0.0049 $\Delta k/k$ increase from 0.0285 to 0.0334 $\Delta k/k$ for the carbide reactor (Tables V and VII). The opposite modes of control rod motion in which the two reactors have to be controlled are responsible for the different increases in sodium void reactivity with burnup.

As mentioned before, the presence of the control poison tends to increase the effect of voiding, because the reactivity worths of control rods decrease when the spectrum hardens. And since the amount of the control poison required to keep the oxide reactor critical decreases with burnup, the contribution of the control poison to the sodium void effect become smaller and smaller for this reactor as burnup progresses. The increase in the sodium void reactivity with burnup for the carbide reactor, on the other hand, is enhanced by an increasing contribution from the control poison. If the core sodium void reactivity of the oxide reactor is to be calculated without control poison all the time, then the increase over the equilibrium cycle would be 0.0042 $\Delta k/k$ instead of only 0.0030 $\Delta k/k$. Similarly, the increase for the carbide reactor, calculated in the same manner, would be reduced to 0.0041 $\Delta k/k$.

Having understood the effect of control poison, the sodium void reactivities of all hypothetical reactors to be analyzed below were calculated in absence of control poison and also in absence of fission products, so that the effects of their presence can be eliminated. However, all these reactors were still assumed to have a zero excess reactivity if they gain reactivity, or to have an excess reactivity equal to the magnitude of the burnup swing if they lose reactivity.

(2) Effects of Sodium Volume Fraction

The fuel, structure, and coolant volume fractions in the core of the original carbide reactor are 0.3757, 0.1427, and 0.4816, respectively, compared to 0.3845, 0.2157, and 0.3848, respectively, for the original oxide reactor. A higher coolant volume fraction is necessary for the carbide reactor because it has a higher linear heat rating than the oxide reactor. The consequences of having different coolant volume fractions on sodium void reactivity can be determined by comparing the sodium void reactivity of this carbide reactor to that of a hypothetical reactor which also uses carbide as fuel but has the same coolant volume fraction as the oxide reactor. In other words, we analyzed an oxide design which, however, uses carbide pellets instead of oxide pellets. The density of those pellets was varied.

Table X shows some important characteristics and sodium void reactivities of four hypothetical carbide reactors, all of which are identical to the oxide reactor in configuration as well as in coolant, fuel and structure volume fractions. The differences among themself are only in the fuel density.

In Case 1, a pellet density equal to that of the original carbide reactor, i.e., 95% T.D. or 12.33 gm/cm^3 is used, and the core sodium void reactivity becomes 0.0236 $\Delta k/k$. This sodium void reactivity is somewhat lower than that of the original carbide reactor (0.0255 $\Delta k/k$), but is still considerably higher than that of the oxide reactor (0.0191 $\Delta k/k$, excluding the effect of control poison). Therefore, the difference in the sodium content for oxide and carbide reactors is not a major factor in the difference in sodium void reactivity.

(3) Effects of Heavy-Metal Concentration

The density of heavy metal in 100% T.D. carbide fuel is 12.98 gm/cm^3, while it is only 9.65 gm/cm^3 in 100% T.D. oxide fuel. Taking into account the difference in the pellet density, the heavy metal concentration in the core for the first hypothetical reactor is $\frac{12.98}{9.65} \times \frac{95\%}{91.4\%} = 1.398$ times that for the original oxide reactor, which has a pellet density of 91.4%. In the three remaining cases shown in Table X, the (carbide) fuel pellet density is reduced to 85 (case 2), 75 (case 3), and 68% T.D. (case 4), respectively. The volume fractions for fuel, coolant, and structure remain the same as in the first case.

The median energy of the neutron flux in the core is higher for lower pellet densities because the reactor requires higher fuel enrichments as the pellet density becomes lower. The number of neutrons leaking out of the core per fission neutron generated in the core increases with decreasing pellet density, and so does its increase due to voiding. This means that the leakage component of the sodium void effect becomes larger as the heavy metal concentration decreases. The η value of the reactor, i.e., the number of fission neutrons released per neutron absorbed in the reactor, increases with decreasing pellet density. However, the increase in η when the core is voided is smaller for lower pellet densities, indicating that the positive spectral component of the sodium void effect becomes smaller when the pellet density is reduced.

The net sodium void reactivity of the core is plotted in Fig. 13 as a function of the pellet density. With a decreasing spectral component and a increasing leakage component, the net sodium void reactivity decreases with decreasing pellet density. Quantitatively, as the pellet density decreases by 28%, from 95 to 68% T.D., the sodium void reactivity decreases by 17%, from 0.0236 to 0.0195 $\Delta k/k$.

The number of heavy metal atoms in the 68% T.D. carbide fuel is equal to that in an equal volume of the 91.4% T.D. oxide fuel. Having the same fuel volume fraction, the Case 4 hypothetical carbide reactor and the original oxide reactor thus have the same heavy metal concentration in their cores. The core sodium void reactivities for these two reactors are extremely close to each other (0.0195 vs. 0.0191 $\Delta k/k$). This is a rather surprising phenomenum because it implies that, as long as the heavy metal concentration and the sodium content remain unchanged, the sodium void reactivity is little affected by the fuel type. It can be so only if the effect of oxygen or carbon or their difference on sodium void reactivity is small.

A parameter frequently considered in analysis of the sodium void reactivity is the fertile-to-fissile ratio. For a given core design and fuel type, the fertile-to-fissile ratio decreases as the pellet density decreases. The sodium void reactivities given in Table X for the different carbide pellet densities, thus, follow the general rule that the sodium void reactivity is larger for a higher fertile-to-fissile ratio than for a lower one. Furthermore, an equal fertile-to-fissile ratio will lead to a practically identical sodium void reactivity for oxide and carbide fuels used in the same design. When the fertile-to-fissile ratio for carbide is extrapolated down to 7.19 (the value for the original oxide reactor), then its sodium void reactivity becomes 0.0190 $\Delta k/k$, which is only about half a percent lower than that for the oxide with the same fertile-to-fissile ratio.

It is interesting to note that, although the sodium void reactivities for those hypothetical reactors with negative reactivity swing were calculated for a initial k_{eff} equal to (1 + magnitude of reactivity swing), it has been shown that they are almost independent of the initial k_{eff}, as long as they are expressed in terms of $\Delta k/k$. For instance, the sodium void reactivity for the case of 68% T.D. pellet density is 0.0194 $\Delta k/k$ if the initial k_{eff} is taken to be unity. This value has a difference of only 0.5% (i.e., 0.0001 $\Delta k/k$) from that calculated for an initial k_{eff} equal to (1 + magnitude of reactivity swing), which is 1.0189.

The difference in the real and adjoint spectra averaged over the first ring of the active core between the original oxide reactor and the Case 1 and 4 hypothetical carbide reactors are presented in Fig. 14 and 15. The real spectra for the two hypothetical reactors are considerably harder than the oxide reactor. But, although the adjoint spectrum for the first hypothetical reactor is harder than the oxide reactor, it is interesting to see that the adjoint spectrum for the fourth hypothetical reactor is practically identical to the oxide reactor. These latter two reactors have the same heavy metal concentration (but different fuel types) and their adjoint fluxes are lower than the first hypothetical carbide at energies above the threshold of ^{238}U fissions (the lower energy boundary of the fourth energy group is about 1.1 MeV).

(4) Effects of Oxygen and Carbon and Their Concentrations

It has been shown that the differences in the type and number of moderating atoms in fuel does not distinctly affect the difference in sodium void reactivity between the oxide and carbide fuels. However, the assumption made is that the sodium and heavy metal concentrations are the same for both reactor types. Such an assumptions, however, is never fulfilled in actual designs. To obtain a more detailed understanding of the impact of the moderating atoms on the sodium void reactivity, the oxygen and carbon concentrations were varied.

Table XI and XII shows the effects of changing the moderator concentration in the original oxide reactor and in the hypothetical carbide reactor with 68% T.D. fuel. Since the heavy metal concentration, along with concentration of other material, is fixed, the moderator concentration is given in number of atoms per heavy metal atom.

For both oxide and carbide fuels, as moderator concentration rises the leakage as well as its increase due to voiding decrease, but, the total sodium void reactivity decreases. For a 50% increase in the moderator concentration, the sodium void reactivity for the oxide fuel decrease by 17%, whereas that for the carbide fuel decreases by 13%. The sodium void reactivity is therefore somewhat more sensitive to oxygen than to carbon concentration. Regardlessly, the changes in either case are not very great.

Figure 16 shows schematically the dependences of the sodium void reactivities for both fuels upon their moderator-to-heavy metal ratio (the oxygen-to-heavy metal ratio of 2:1 is lined with the carbon-to-heavy metal ratio of 1:1). One important point to notice is that these two fuels approach each other in sodium void reactivity at low moderator-to-heavy metal ratios, and the difference between them becomes greater as the oxygen and carbon concentrations become higher. In other words, the difference in the effects of carbon and oxygen atoms, becomes more apparent, when there are more of these atoms in the reactor. However, even for the highest oxygen- and carbon-to-heavy metal ratios analyzed (2.4:1 and 1.2:1 respectively), the difference in sodium void reactivity between these two types of fuel is still insignificant. The increase in the difference is much smaller than the changes in the respective sodium void reactivities when the oxygen- and carbon-to-heavy metal ratios increase. Therefore, one can conclude that an oxide and a carbide reactors with the same heavy metal concentration and the same sodium volume fraction have practically the same sodium void reactivity. The effects of oxygen and carbon concentration on sodium void reactivity are small.

V. DOPPLER COEFFICIENTS

The reactivity feedback due to temperature changes presented here includes Doppler broadenings of all isotopes whose mass numbers are greater than 100. These include all fissile and fertile nuclides. Considerations are given to temperature changes of individual reactor regions as well as the reactor as a whole. The effects of sodium voiding on Doppler reactivities are also presented. The term "total Doppler coefficient" of a reactor used below refers to the reactivity effect of changing the temperature of the entire reactor.

A. Oxide Reactor

The Doppler coefficient for the entire oxide reactor has been analyzed for a temperature range of 650 → 2200°K. For the simplicity of calculations, the reactor is assumed to have a uniform fuel temperature throughout the core and blankets. The total Doppler coefficient for the reactor is then determined by calculating variations in the reactor eigenvalue when this uniform fuel temperature is altered. Table XIII shows that the total Doppler coefficients at BOL, BOEC, and EOEC, averaged over the temperature range, are -109.5, -103.5, and -105.7×10^{-4}, respectively, when the core is flooded, or -79.2, -74.4, and -76.9×10^{-4}, respectively, when the core is voided.

Beside the Doppler coefficient for the entire reactor, the Doppler coefficients for individual region have also been calculated for the temperature range from 1300 → 2200°K. In these calculations the fuel temperature is varied non-uniformly. Starting with a uniform reference temperature of 1300°K, the fuel temperature of the inner core is raised to 2200°K first. The same temperature rise is then extended to the outer core, then to the axial blanket, and finally to the radial blanket. This approach is by no means a good simulation of an actual temperature excursion. Nevertheless, it can provide a way of determining the Doppler coefficients of the various reactor regions. Specifically, the difference in eigenvalue between before and after the fuel temperature of a certain region is raised can be used to calculate the Doppler contribution of that region. The Doppler coefficients for all regions based on this approach are given in Table XIV and XV. Table XIV shows data for a core with sodium and Table XV shows data for a completely voided core.

For a flooded core the Doppler coefficient for the inner core zone is -72.6, -65.2, -66.3×10^{-4}, respectively, at BOL, BOEC, and EOEC. The contribution of the outer core zone is -22.2, -21.4, and -19.5×10^{-4}, respectively, and is slightly less than one-third of that of the inner core zone at the respective stage. The sum of the two core zones accounts for 91 to 85% of the Doppler coefficient for the entire reactor, which is -104.3, -98.4, and -100.6×10^{-4}, respectively, for the current temperature range. The remaining contributions come mainly from the axial blanket.

The Doppler coefficient for the entire reactor for a voided core is about 30% lower than that for a flooded core. The difference comes almost entirely from the core region, where the sodium content is being altered. The variation with burnup of the Doppler reactivity for individual regions follows the same trend for both flooded and voided conditions.

Comparing the total Doppler coefficients for the 1300 → 2200°K temperature range (Tables XIV and XV) with those for the 650 → 2200°K temperature range (Table XIII), one can see that the Doppler reactivity feedback is somewhat larger at lower temperatures.

The Doppler coefficients at BOL based on first order perturbation calculations are given in Table XVI in comparison with the results of direct eigenvalue calculations. Unlike in the calculations of sodium void reactivity, the first order perturbation theory can be applied to the calculations of Doppler coefficient fairly accurately because the magnitudes of reactivity perturbations are now much smaller. For example, the Doppler coefficient for the flooded core is -98.7×10^{-4} based on perturbation calculations, compared to -94.8×10^{-4} based on direct eigenvalue calculations.

B. Carbide Reactor

The total Doppler coefficients for the carbide reactor at different stages, averaged over the 650 → 2200°K temperature range, are listed in Table XVII. When the core is flooded with sodium, the total Doppler coefficient is -110.0, -104.2, and -85.8×10^{-4}, respectively, at BOL, BOEC, and EOEC. They decrease to -71.9, 69.6, and 59.4×10^{-4}, respectively, when the sodium in the core is removed.

The regional contributions to the Doppler reactivity are summarized in Tables XVIII and XIX. The same approach used to determine the regional contributions for the oxide reactor are employed, with the exception of the use of a different temperature range, i.e., 1100 → 2200°K. As in the case of the oxide reactor, the inner core has the largest contribution. If there is sodium in the core, the Doppler coefficient for the inner core is -78.9, -71.8, and -55.8×10^{-4}, respectively, and that of the outer core is -19.9, -19.4, and -17.2×10^{-4}, respectively, at BOL, BOEC, and EOEC. Together, the two core zones contribute about 74 to 67% to the total, which decreases from -106.5×10^{-4} at BOL, to -100.8×10^{-4} at BOEC, then to -83.2×10^{-4} at EOEC. The Doppler coefficient for the entire reactor is reduced by about one-third when the core is voided. The reduction comes mainly from the core.

C. Oxide Reactor vs. Carbide Reactor

As a general rule, the reactivity effect resulting from Doppler broadening of fission and capture resonances is greater for a reactor with a softer neutron spectrum. It is so because cross section variations with temperature are larger at low energies than at high energies. The carbide reactor of this study has a considerably harder spectrum than the oxide reactor (Table IX). However, its Doppler coefficient is about the same as the oxide reactor at BOL (and at BOEC) (TABLE XIV and XVIII). There are two explanations for this phenomenum. First, the carbide reactor has a higher fertile-to-fissile ratio (lower fuel enrichments) in the core than the oxide reactor. This means that for every fissile atom there are more fertile atoms in the carbide reactor than in the oxide reactor, and as a consequence, the carbide reactor tends to have a more negative Doppler coefficient than the oxide reactor, if the neutron spectra are the same. The second explanation is that the carbide reactor has a higher heavy metal concentration. The heavy metal (pellet) density in the core of the carbide reactor is 12.33 gm/cm^3 (95% T.D.), compared to

8.82 gm/cm^3 (91.4% T.D.) in the oxide reactor. Allowing for the difference in the fuel volume fraction, the heavy metal concentration in the carbide reactor is $\frac{12.33}{8.82} * \frac{0.3757}{0.3845} = 1.37$ times higher than in the oxide reactor.

It should be pointed out that the effects of heavy metal concentration and of fuel enrichments on the Doppler coefficient are correlated. An increase in heavy metal concentration results in a decrease in fuel enrichments. And, increasing heavy metal density and decreasing fuel enrichments both tend to make the Doppler coefficient more negative.

In order to quantify the effects of changing heavy metal concentration, the Doppler coefficients of two of the hypothetical carbide reactors discussed in Section IV in demonstrating the effects of the fuel density on sodium voiding (Cases 1 and 4, Table X) are analyzed. Remember that, except for the fuel, these two reactors are identical to the original oxide reactor. In one case the heavy metal density is set equal to the original carbide reactor (12.33 gm/cm^3), and in the other case equal to the original oxide reactor (8.82 gm/cm^3).

The Doppler coefficients, fertile-to-fissile ratios, and the mediam energies of the neutron fluxes in the cores of these two hypothetical reactors as well as the original oxide and carbide reactors are given in Table XX. The hypothetical reactor with 12.33 gm/cm^3 heavy-metal density and the original carbide reactor have about the same fertile-to-fissile ratio (9.55 vs. 9.42) and median flux energy (1.51 vs. 1.54 $\times$ 10^5 eV) and consequently have about the same Doppler coefficient (-98.6 vs. -98.8 $\times$ 10^{-4} for the 1100 $\rightarrow$ 2200°K temperature range). As the heavy metal density of the hypothetical carbide reactor is reduced from 12.33 gm/cm^3 to 8.82 gm/cm^3, the fertile-to-fissile ratio is reduced from 9.55 to 7.42, and the core Doppler coefficient is reduced from -98.6 to -83.8 $\times$ 10^{-4}, though the median flux energy increases only slightly. The original oxide core has a fertile-to-fissile ratio slightly lower than the hypothetical carbide core of the same heavy metal density (8.82 gm/cm^3). However, the Doppler coefficient is higher for the former because it has a median energy significantly lower than that the latter has.

Although showing little difference at BOL and BOEC, the Doppler coefficients for the original oxide and carbide reactors react to burnup quite differently. The Doppler coefficient for the oxide reactor shows very little change, whereas that for the carbide reactor decreases significantly over the equilibrium cycle (Tables XIV and XVIII). The decrease in the Doppler with burnup for the carbide reactor comes mainly from the decrease in the contribution of the inner core zone, where the temperature reactivity effect is largest.

It is shown in Section III that the conversion ratio in the inner core of the oxide reactor is close to and somewhat below unity (Table II). Because of such a conversion ratio, the fertile-to-fissile ratio in the inner core is little affected by burnup, changing only from 8.01 at BOEC to 7.81 at EOEC. Furthermore, the effect on Doppler of this slight decrease in fertile-to-fissile ratio is offset somewhat by the slight softening of the neutron spectrum. As a result, the Doppler coefficient for the oxide reactor show only small changes with burnup. The conversion ratio in the inner core of

the carbide reactor, on the other hand, is significantly greater than unity (Table IV). Its fertile-to-fissile ratio decreases more significantly (from 10.46 to 9.58) over the equilibrium cycle. In addition, the neutron spectrum in this core becomes slightly harder as burnup increases. Therefore, the Doppler coefficient for the carbide reactor is more dependent on burnup than that for the oxide reactor. Its core Doppler coefficient decreases by 20%, from -91.2 to 73.0 $\times 10^{-4}$, over the equilibrium cycle.

VI. SUMMARIES AND CONCLUSIONS

The negative leakage components of the sodium void effects in the oxide and carbide reactors investigated here are dominated by the positive spectral components, and the sodium void reactivities are large and positive for both reactors. The sodium void reactivities become even more positive when fission products build up. Of the two reactors, the carbide reactor has the more positive sodium void effect. The increase in the sodium void reactivity with burnup is also larger for the carbide reactor. The comparative analyses of the sodium void effects of these two and some hypothetical reactors lead to the following conclusions:

(1) The presence of control poison enhances the sodium void effect of a reactor

(2) Because the amount of control poison needed for criticality increases more quickly for a reactor with a more positive burnup swing, the more positive the burnup swing, the larger the increase in the sodium void reactivity over a burn cycle.

(3) The major source of difference in the sodium void reactivity between an oxide and a carbide reactor is the difference in their heavy metal concentrations. For realistic designs, a carbide reactor usually has a higher heavy metal concentration and a larger sodium void reactivity than an oxide reactor of the same power output.

(4) The heavy metal concentration affects the sodium void reactivity mainly because it determines the fertile-to-fissile ratio of a reactor which in turn determines the spectral effect of voiding.

(5) For a fixed heavy metal concentration and a fixed coolant volume fraction, the sodium void reactivity is almost independent of the type of fuel used, carbide or oxide, and is fairly insentive to the concentration of moderating atoms.

(6) The difference in the sodium volume fraction between an oxide and a carbide reactor also affects their sodium void reactivities, but it is not a major factor.

(7) Although the fuel type does not affect the sodium void reactivity directly, the selection of fuel dictates such parameters as the fuel density and coolant volume fraction that influence the sodium void reactivity directly.

The Doppler effect is influenced by many factors. Generally speaking, a softer spectrum, a higher fertile-to-fissile ratio, and a higher heavy metal concentration would lead to a larger negative Doppler reactivity feedback. The carbide reactor investigated has a higher fertile-to-fissile ratio and a higher heavy metal concentration, but its spectrum is harder than the oxide reactor. The Doppler coefficients of the two reactors are comparable at the beginning of life as well as at the beginning of equilibrium cycle when there are no or few fission products in the reactors. The Doppler coefficient of the oxide reactor remains relatively unchanged with burnup, but that of the carbide reactor is greatly reduced when the fuel irradiation increases. These different responses to burnup are caused primarily by the different inner-core conversion ratios of the two reactors which determine how the fertile-to-fissile ratios in the inner cores change with burnup.

APPENDIX

Integral Sodium Void Reactivities

The core sodium void reactivities presented in Section IV (Tables V and VII) for two 3000 MWth LMFBRs are integral data. Although large and positive, they include negative contributions from the outer parts of the cores. If these negative contributions are excluded, the core sodium void reactivities would be somewhat higher than the values given in Section IV.

The term "integral sodium void reactivity" used here refers to that for a region extending from the core centerline to an arbitrary radius R within the core (with the control rod channels excluded). Axially, this region covers the entire active core height.

The integral sodium void reactivity so defined for the oxide core at BOL is plotted as a function of the radius in Fig. 17, where the results of the direct eigenvalue and perturbation calculations are both illustrated. The curve for the perturbation approach is consistently lower than that for the direct approach. The maximum of the former is 0.0194 $\Delta k/k$ and appears at $R = 164 \pm 4$ cm, i.e., about 15 cm from the edge of the core. The uncertainity of ± 4 cm is due to finite mesh sizes.

The maximum from the direct approach is 0.0212 $\Delta k/k$. This value is 4.4% higher than that for the entire core, which is 0.0203 $\Delta k/k$. The location of the maximum from the direct approach agrees with the perturbation approach within the ± 4 cm range, because the value at 164 cm is greater than the values at 160 or 168 cm. The differences among the values at these three locations, however, are almost negligible (within 1%).

The integral sodium void reactivity for the carbide core is shown in Fig. 18. The maximum from the direct and perturbation approaches are 0.0267 and 0.0258 $\Delta k/k$, respectively. They both appear at $R = 146 \pm 4$ cm, about 14 cm from the core-radial blanket interface. The maximum integral sodium void reactivity based on the direct eigenvalue calculations, is 4.7% higher than the sodium void reactivity of the entire core of 0.0255 $\Delta k/k$.

REFERENCES

1. H. H. Hummel and D. Okrent, "Reactivity Coefficients in Large Fast Power Reactors," Monograph Series on Nuclear Science and Technology, American Nuclear Society (1970).

2. T. A. Daly, G. K. Leaf, and A. S. Kennedy, "The ARC System Two-dimensional Diffusion Theory Capability, DARC2D," ANL-7716, Argonne National Laboratory (May 1972).

3. R. P. Hosteny, private communication (1976).

4. H. Henryson II, B. J. Toppel, and C. G. Stenberg, "MC^2-2: A Code to Calculate Fast Neutron Spectra and Multigroup Cross Sections," ANL-8144, Argonne National Laboratory (June 1976).

5. H. Henryson II et al., private communication (May 1972).

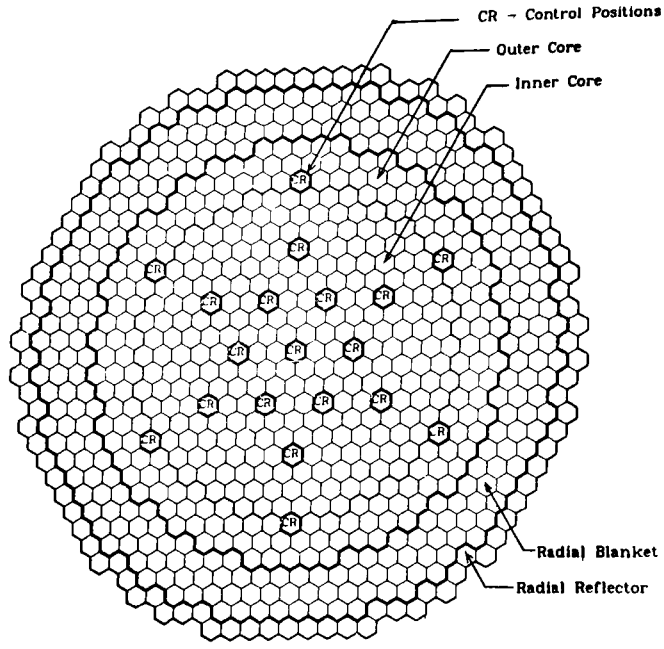

Zone	Number of Assemblies
Core	402
Radial Blanket	252
Radial Reflector	96
Control Positions	19

Fig. 1. Configuration of 3000 MWth Oxide LMFBR

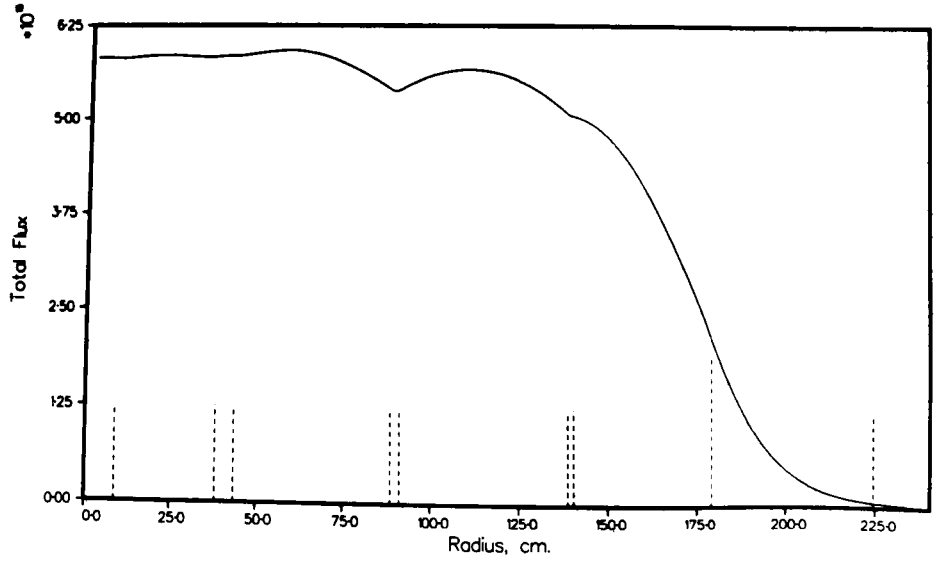

Fig. 2a. Total Flux Distribution at Mid-Plane of Oxide Reactor (BOL)

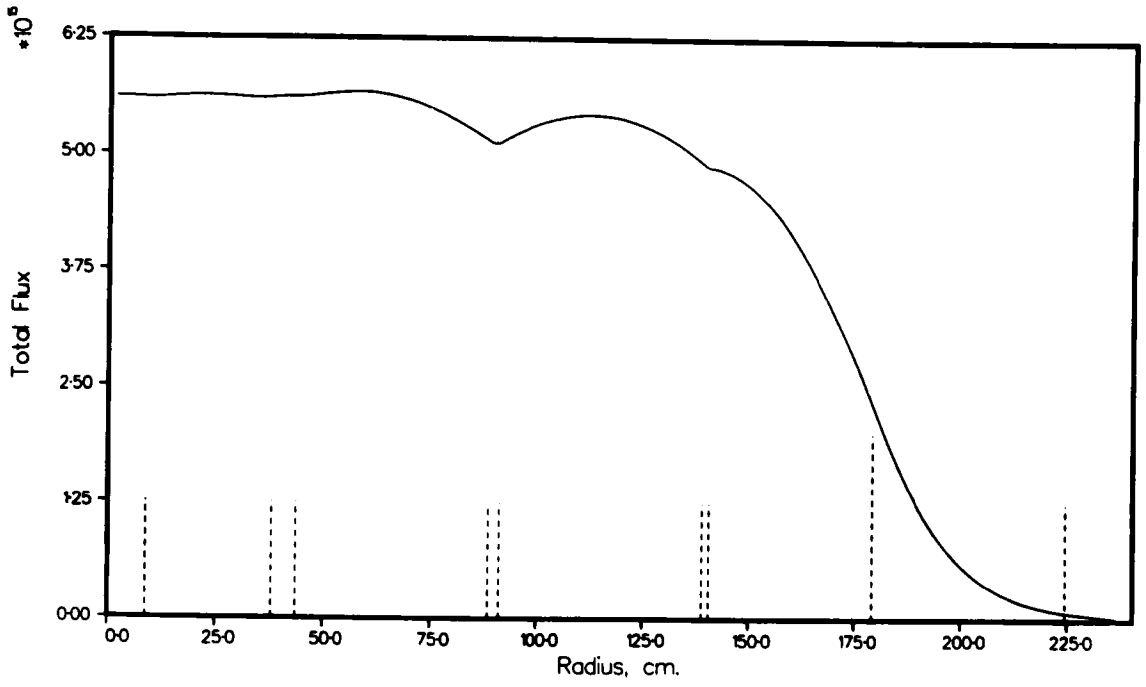

Fig. 2b. Total Flux Distribution at Mid-Plane of Oxide Reactor (BOEC)

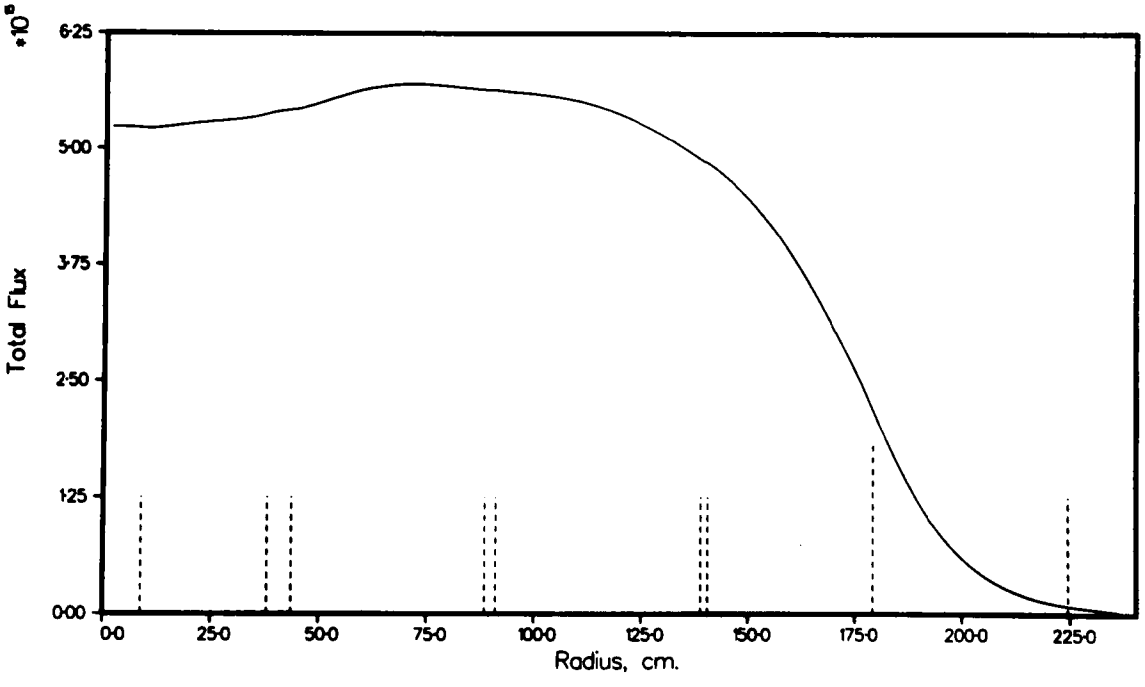

Fig. 2c. Total Flux Distribution at Mid-Plane of Oxide Reactor (EOEC)

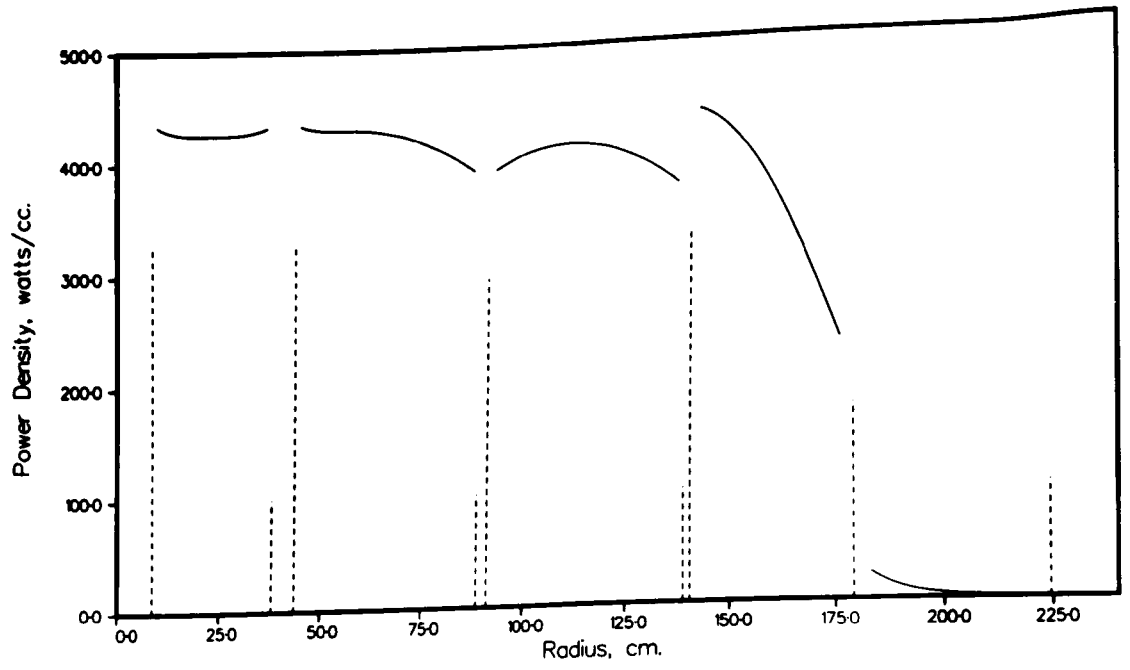

Fig. 3a. Power Distribution at Mid-Plane of Oxide Reactor (BOL)

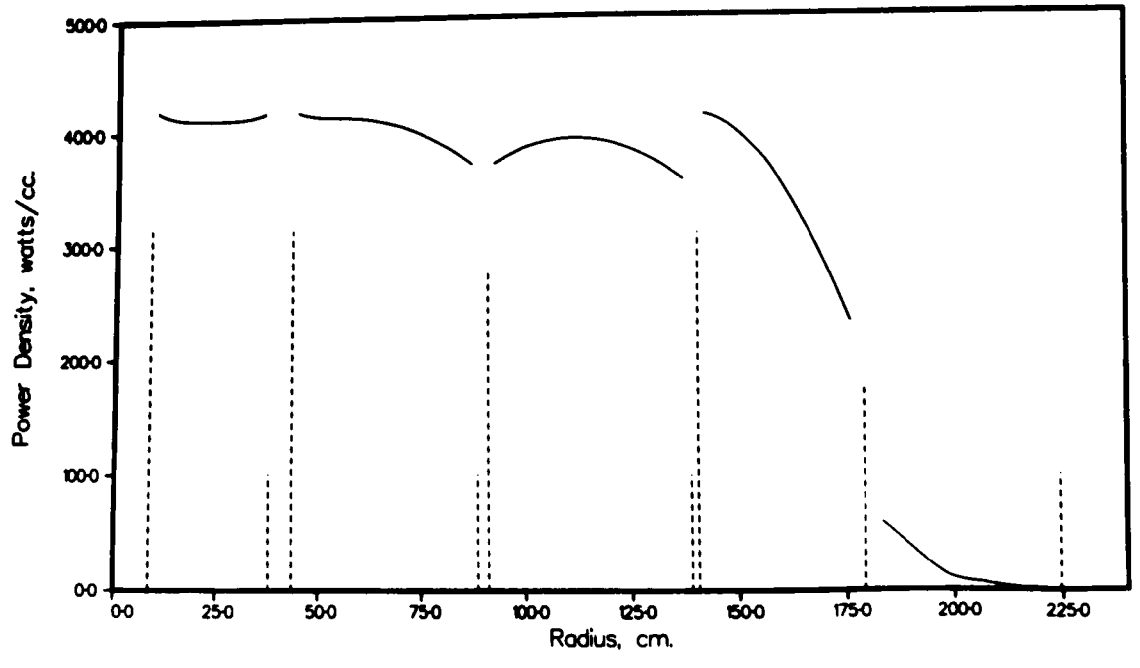

Fig. 3b. Power Distribution at Mid-Plane of Oxide Reactor (BOEC)

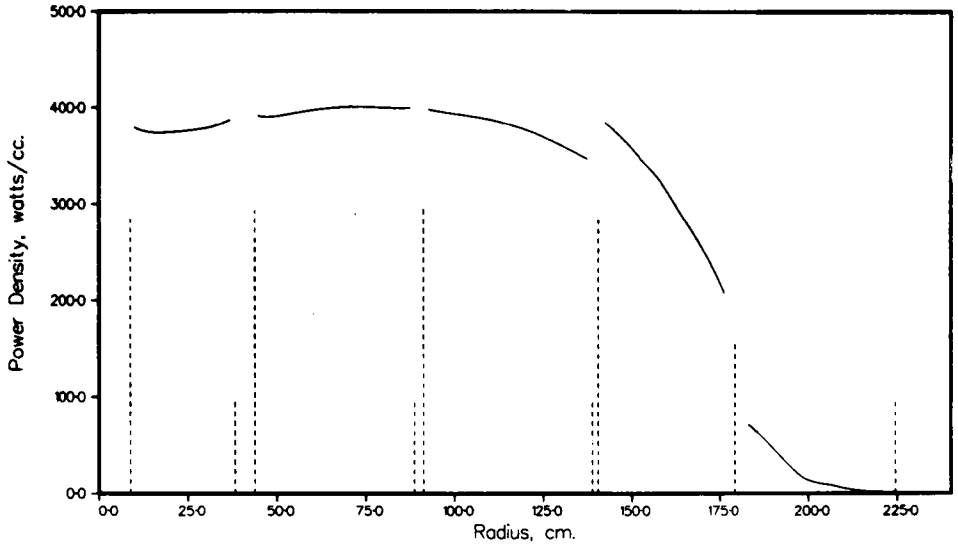

Fig. 3c. Power Distribution at Mid-Plane of Oxide Reactor (EOEC)

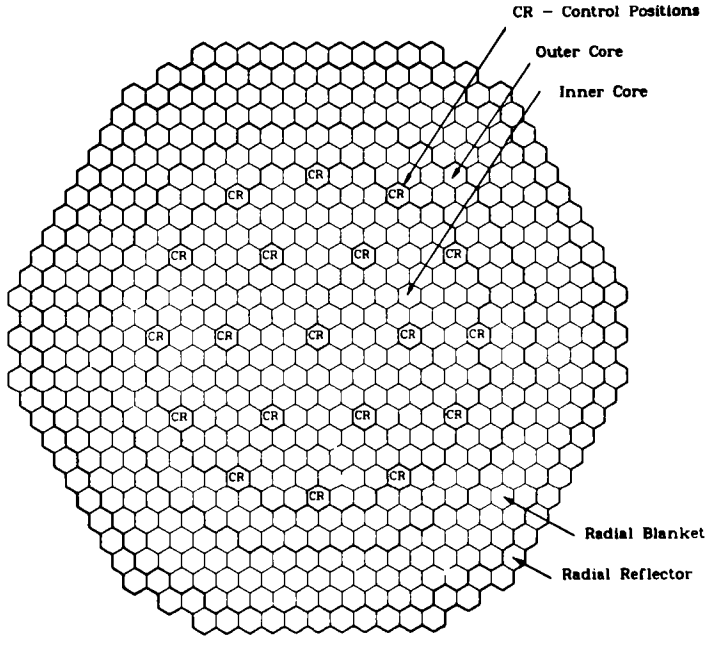

Zone	Number of Assemblies
Core	294
Radial Blanket	216
Radial Reflector	84
Control Positions	19

Fig. 4. Configuration of 3000 MWth Carbide LMFBR

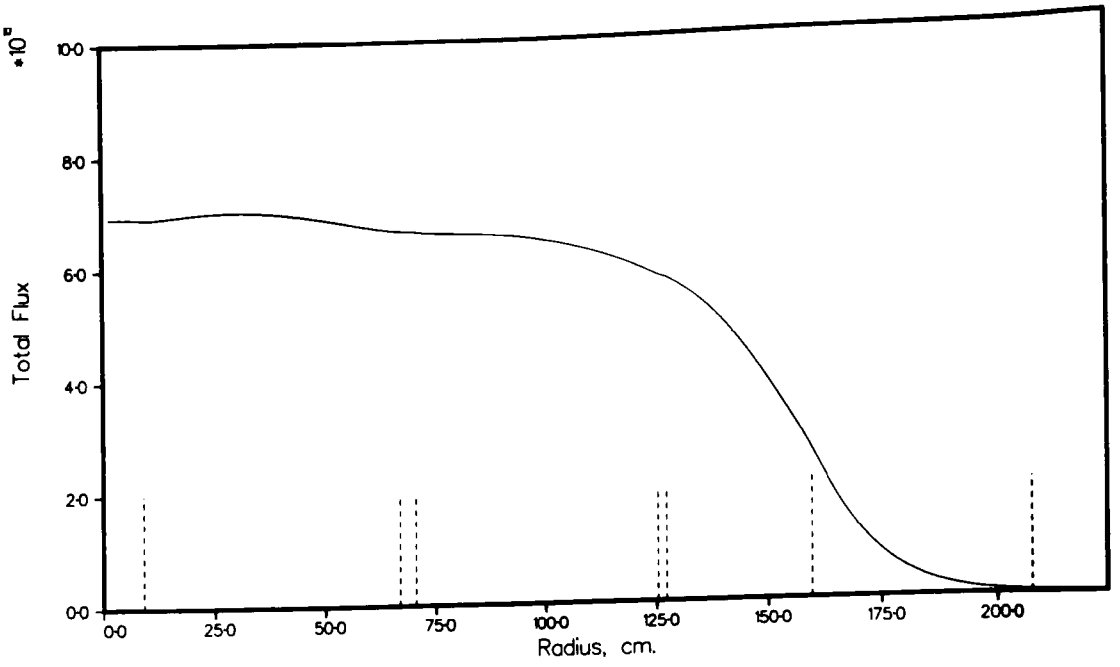

Fig. 5a. Total Flux Distribution at Mid-Plane of Carbide Reactor (BOL)

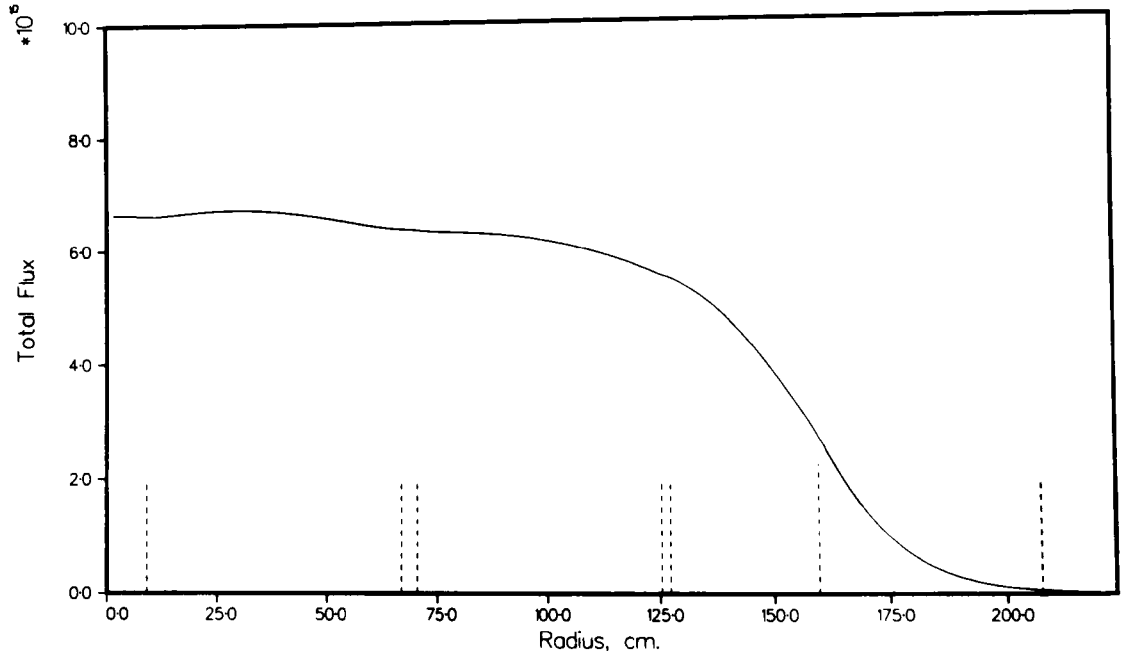

Fig. 5b. Total Flux Distribution at Mid-Plane of Carbide Reactor (BOEC)

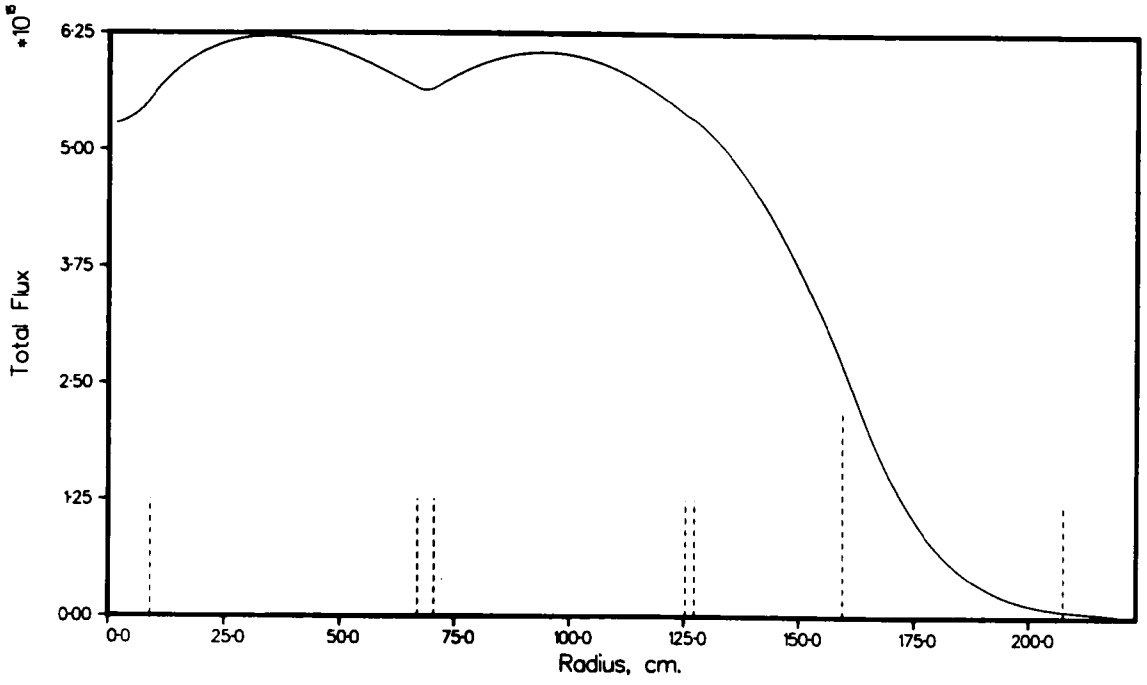

Fig. 5c. Total Flux Distribution at Mid-Plane of Carbide Reactor (EOEC)

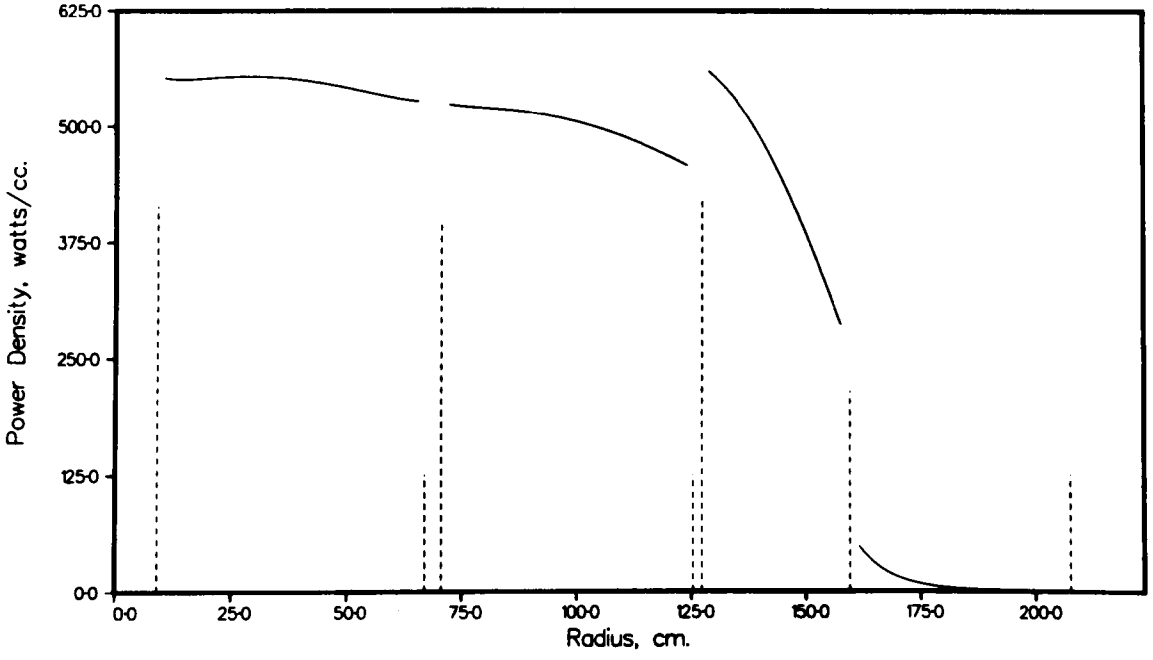

Fig. 6a. Power Distribution at Mid-Plane of Carbide Reactor (BOL)

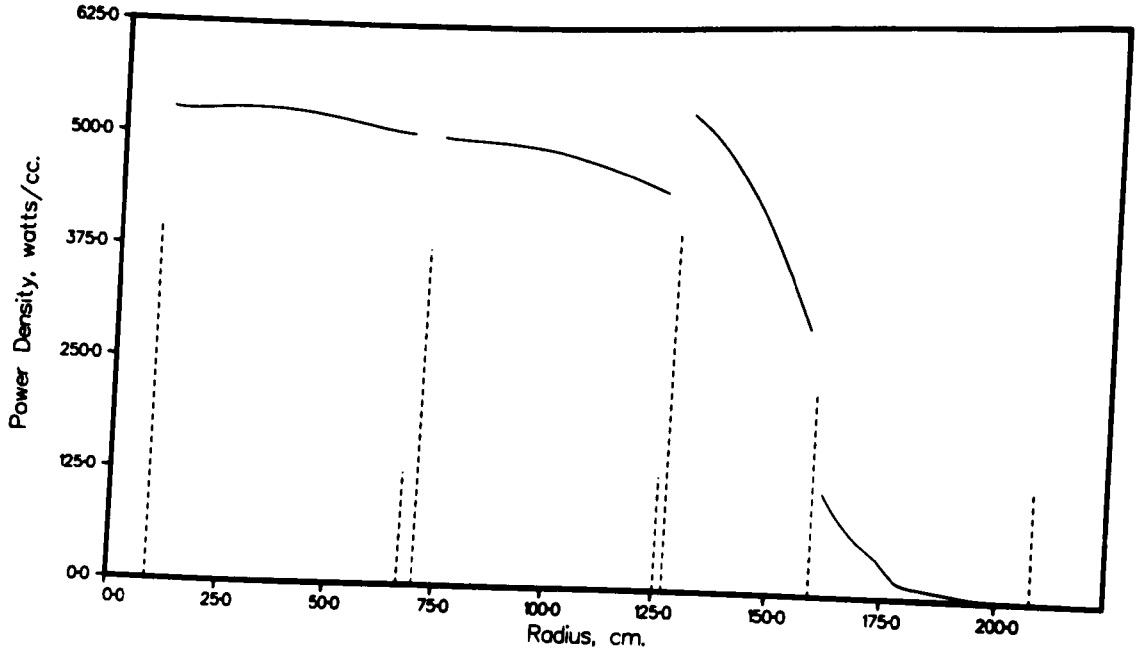

Fig. 6b. Power Distribution at Mid-Plane of Carbide Reactor (BOEC)

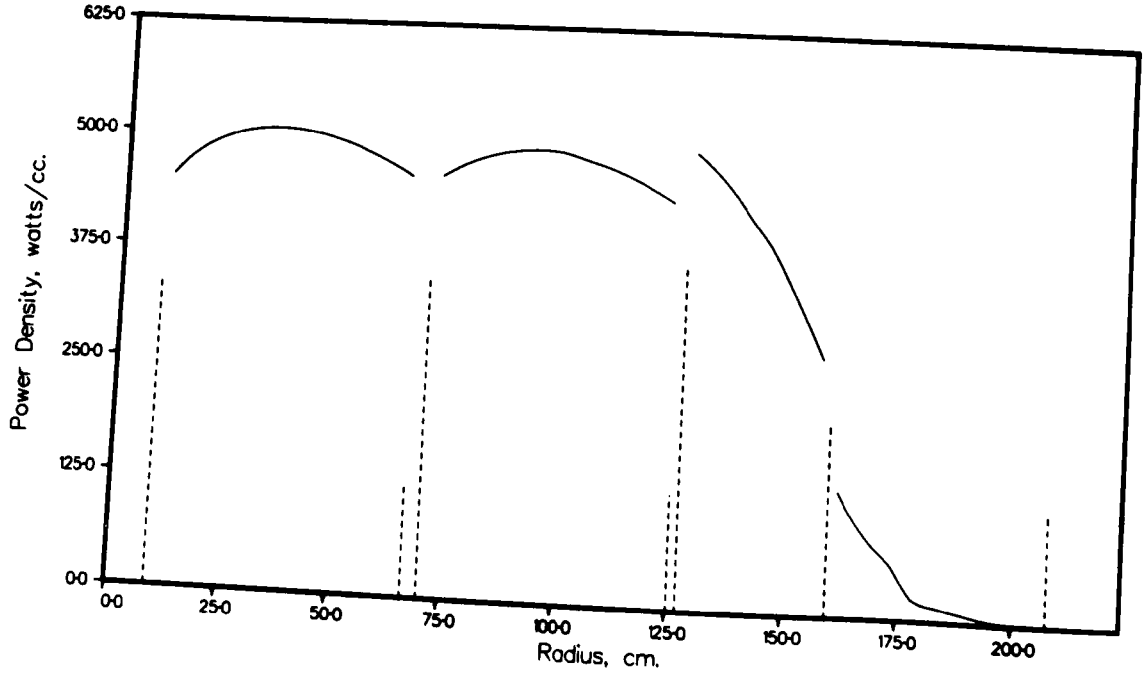

Fig. 6c. Power Distribution at Mid-Plane of Carbide Reactor (EOEC)

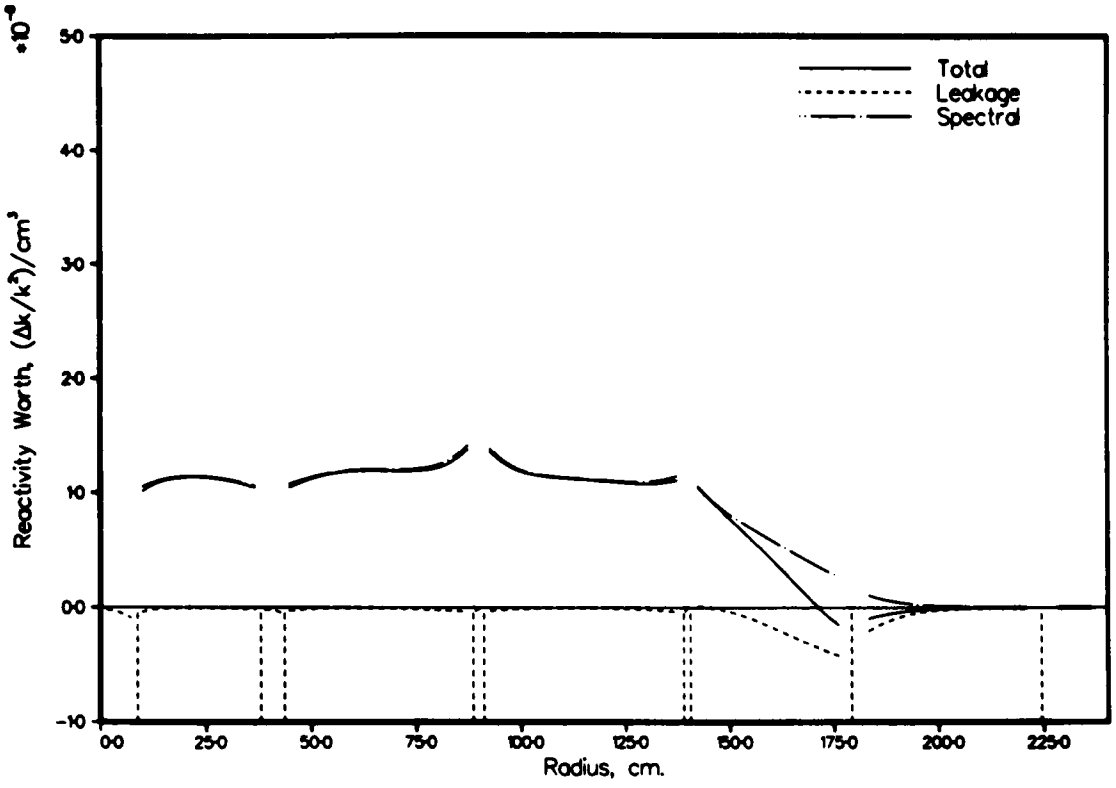

Fig. 7a. Radial Variation of Sodium Void Reactivity in Oxide Reactor at BOL (at Mid-Plane)

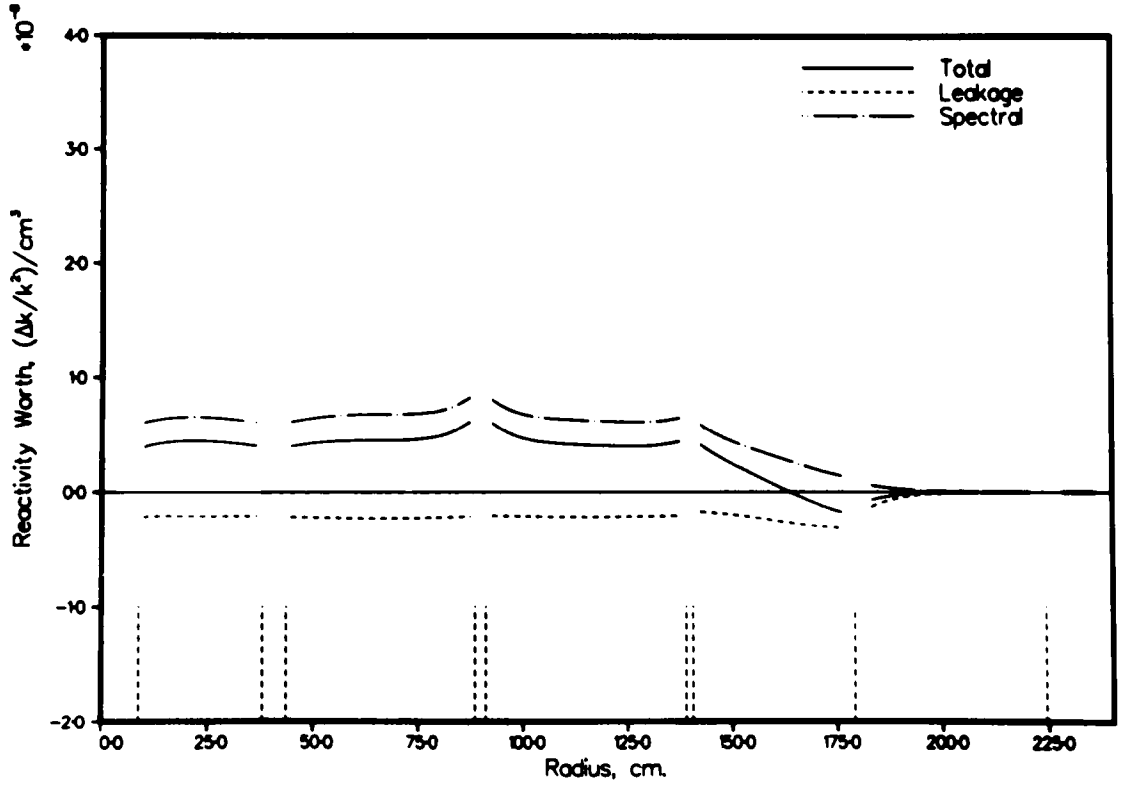

Fig. 7b. Radial Variation on Sodium Void Reactivity in Oxide Reactor at BOL (at 30 cm from Mid-Plane)

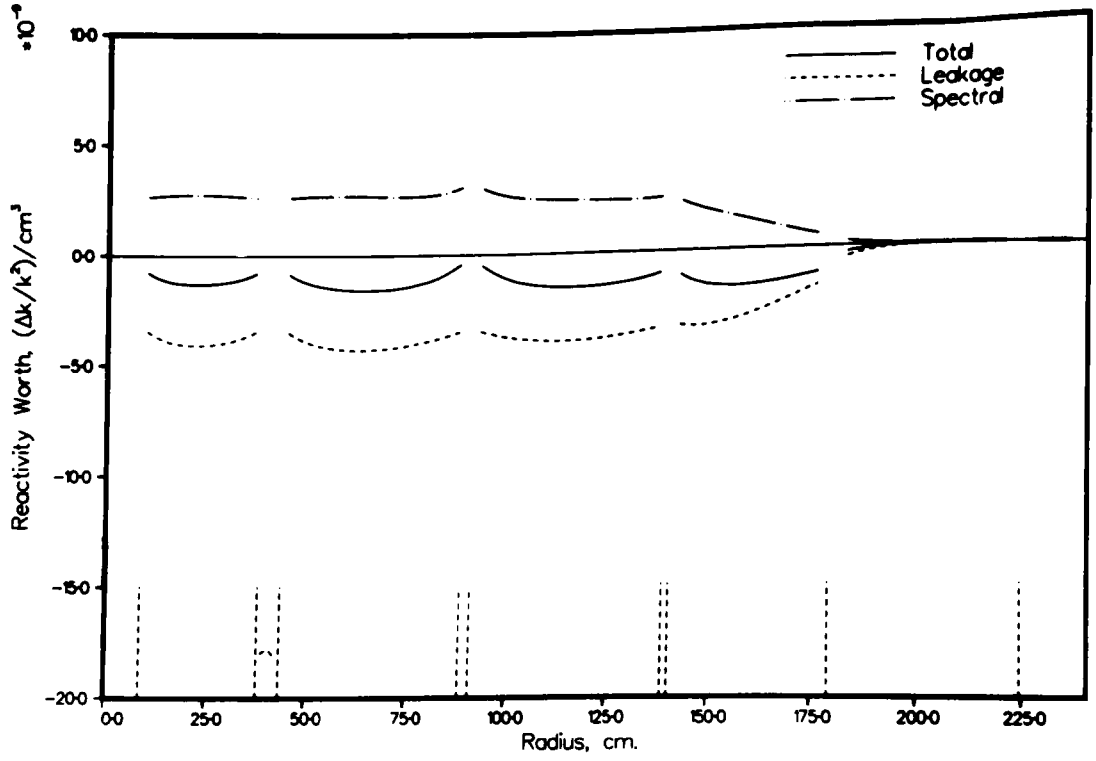

Fig. 7c. Radial Variation of Sodium Void Reactivity in Oxide Reactor at BOL (at 49 cm from Mid-Plane)

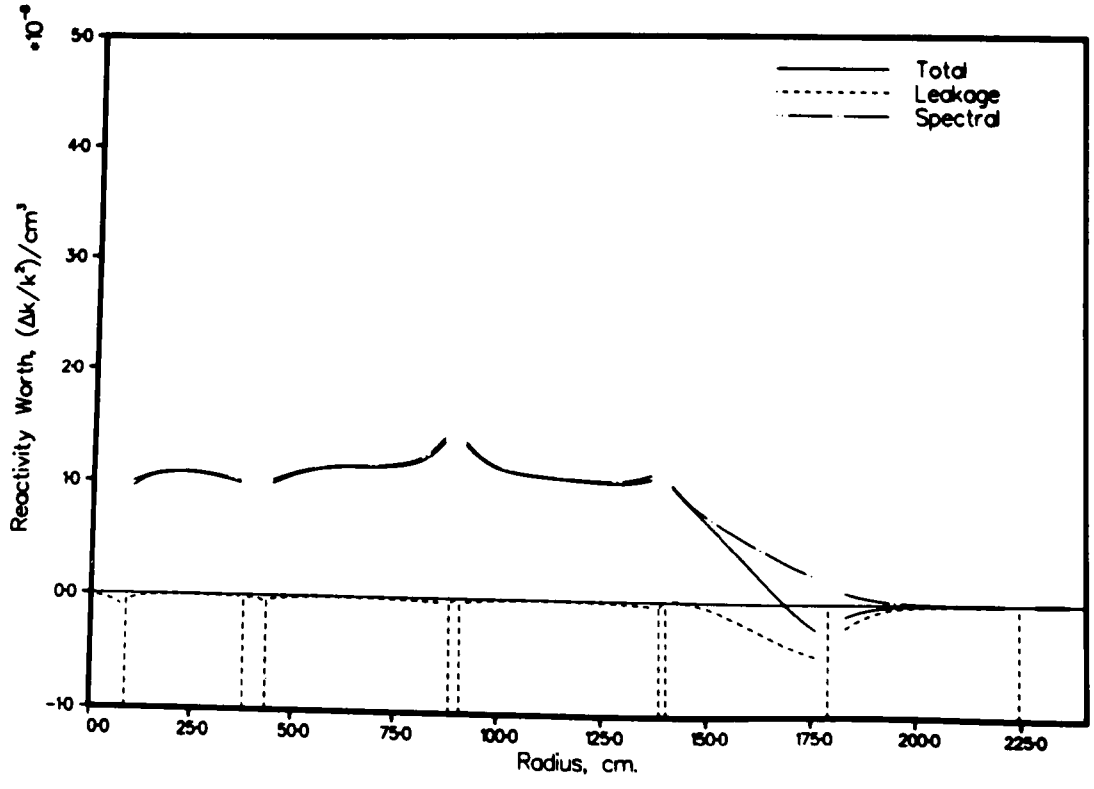

Fig. 8a. Radial Variation of Sodium Void Reactivity in Oxide Reactor at BOEC (at Mid-Plane)

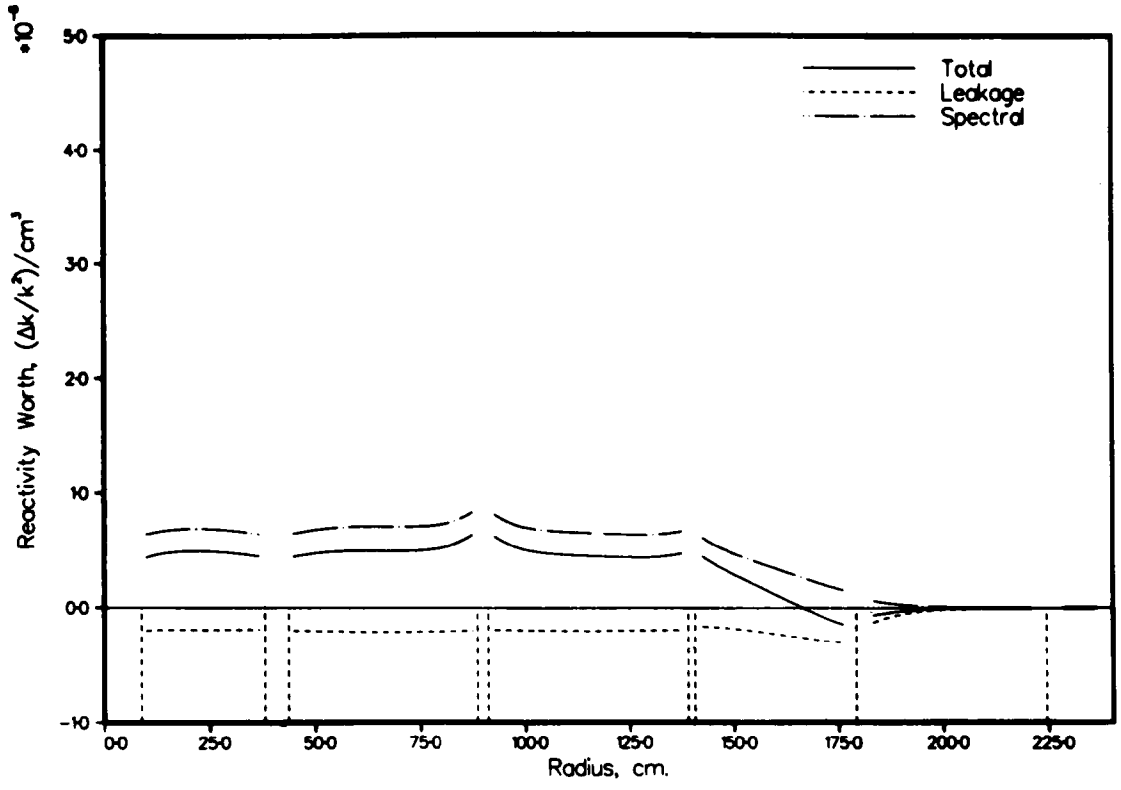

Fig. 8b. Radial Variation of Sodium Void Reactivity in Oxide Reactor at BOEC (at 30 cm from Mid-Plane)

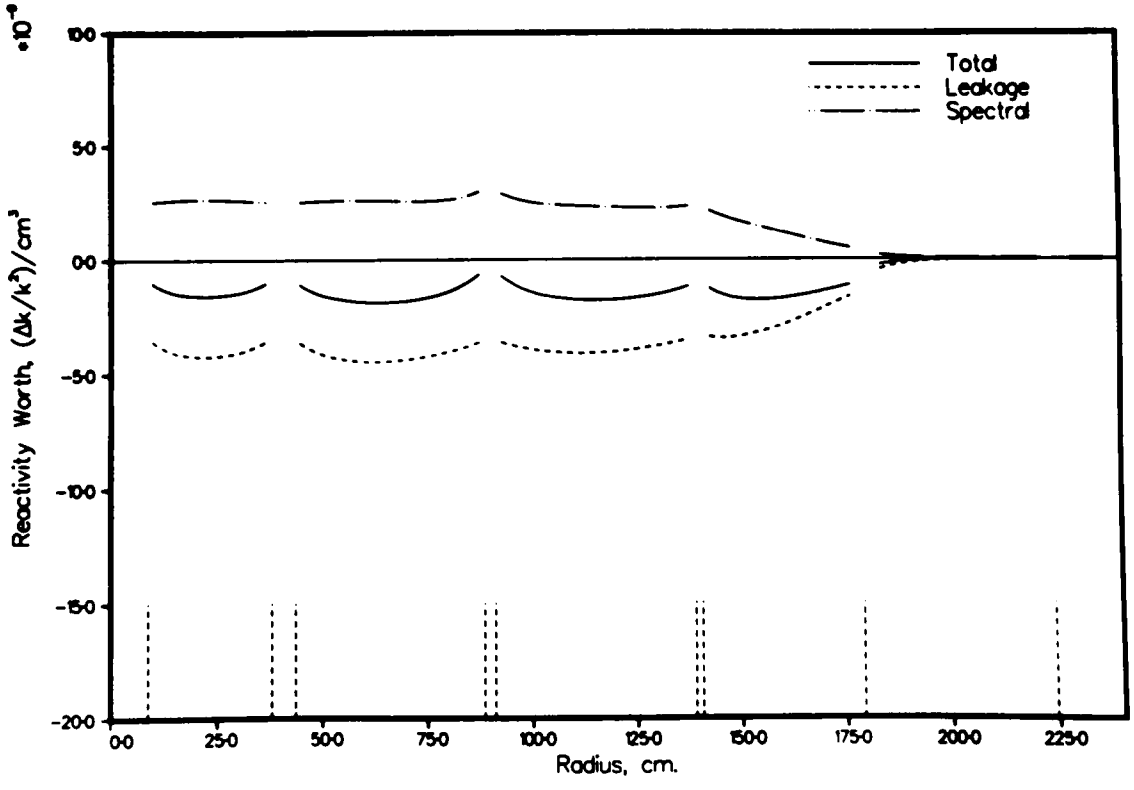

Fig. 8c. Radial Variation of Sodium Void Reactivity in Oxide Reactor at BOEC (at 49 cm from Mid-Plane)

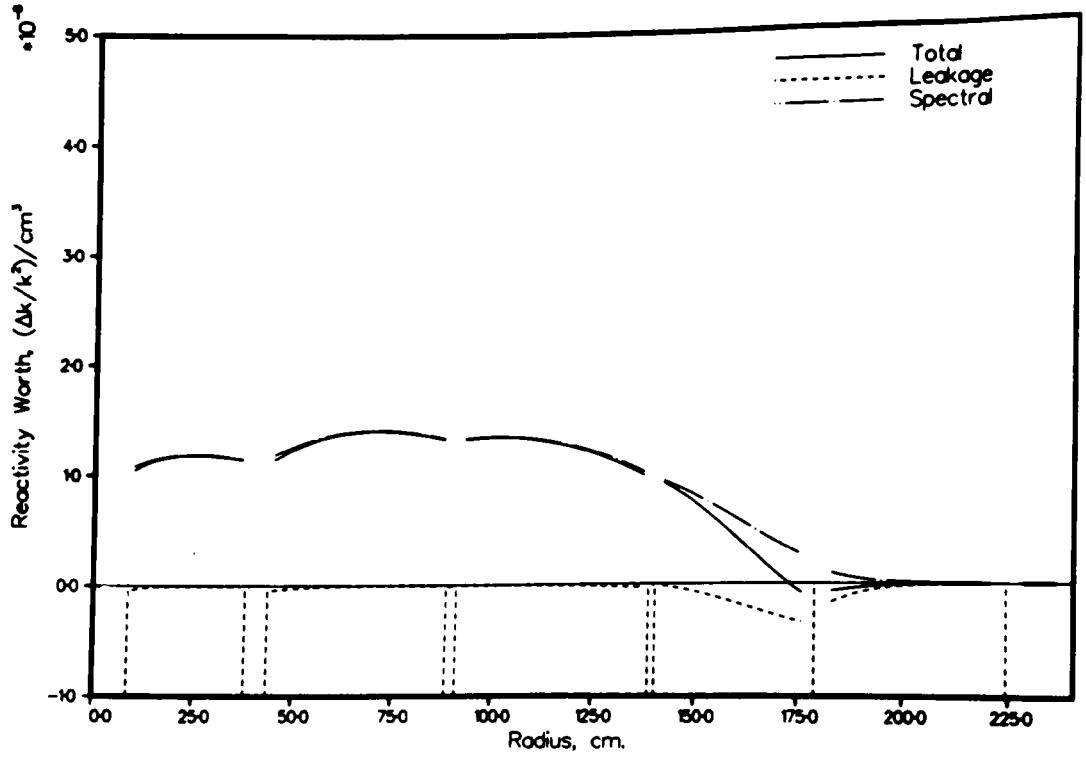

Fig. 9a. Radial Variation of Sodium Void Reactivity in Oxide Reactor at EOEC (at Mid-Plane)

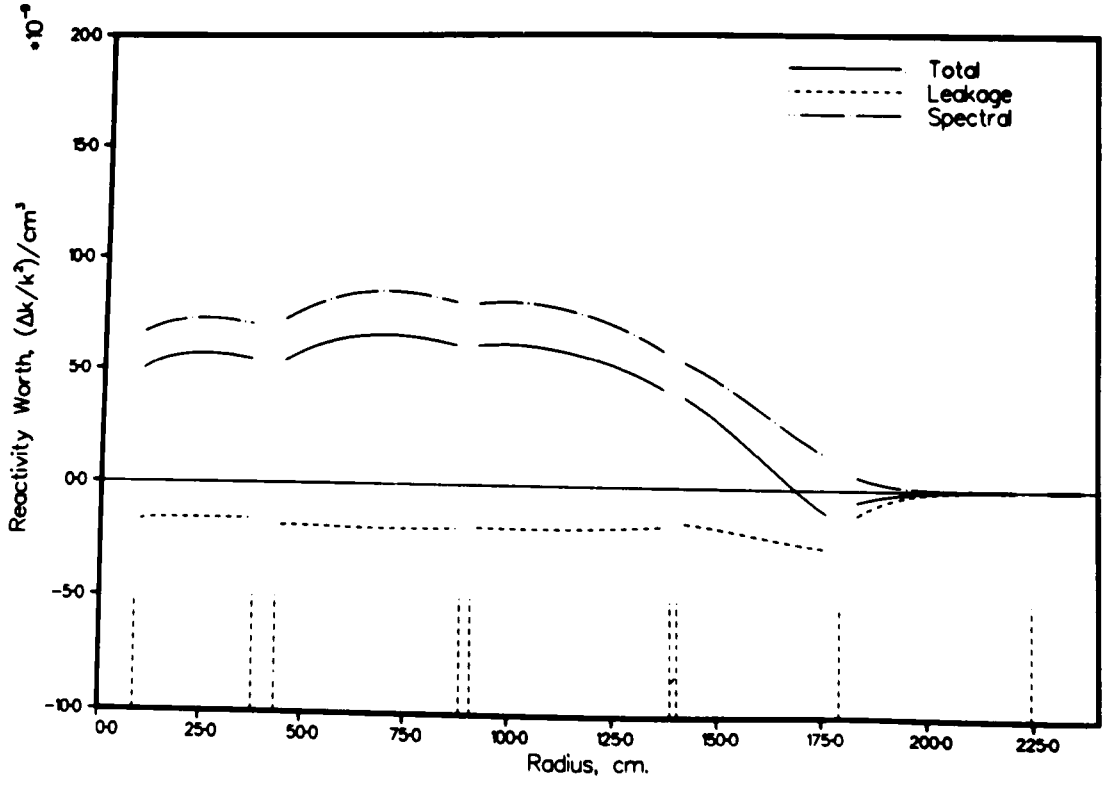

Fig. 9b. Radial Variation of Sodium Void Reactivity in Oxide Reactor at EOEC (at 30 cm from Mid-Plane)

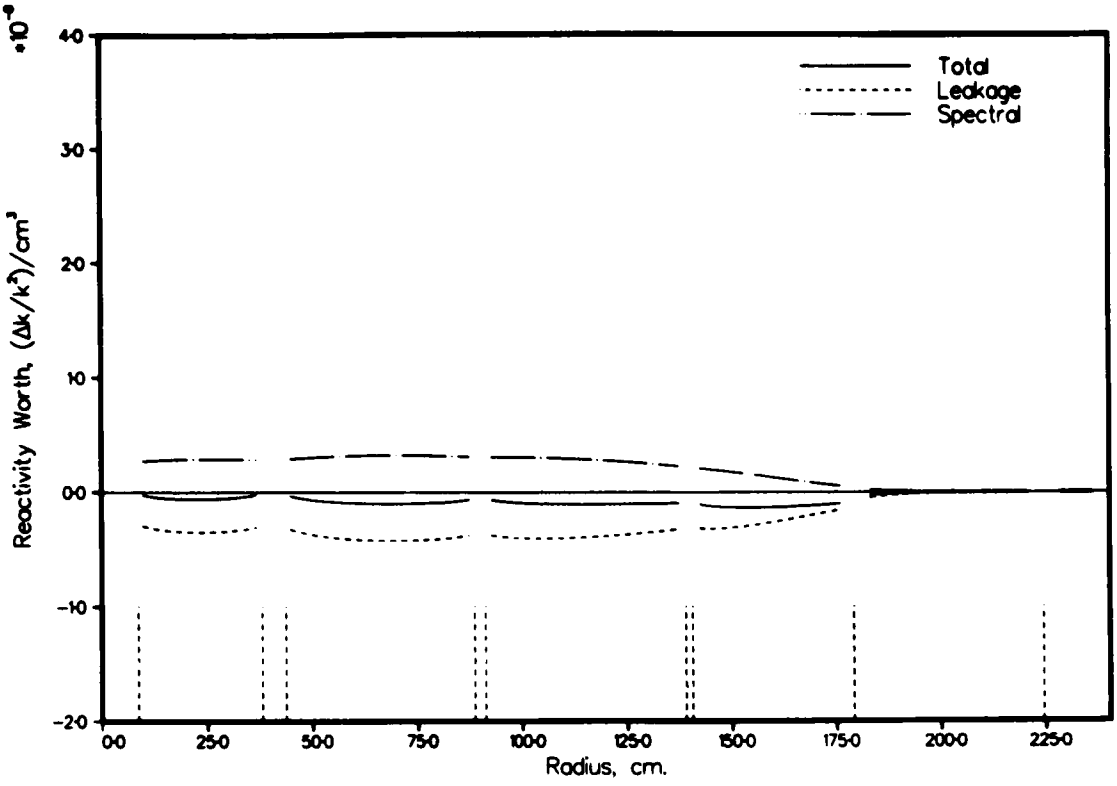

Fig. 9c. Radial Variation of Sodium Void Reactivity in Oxide Reactor at EOEC (at 49 cm from Mid-Plane)

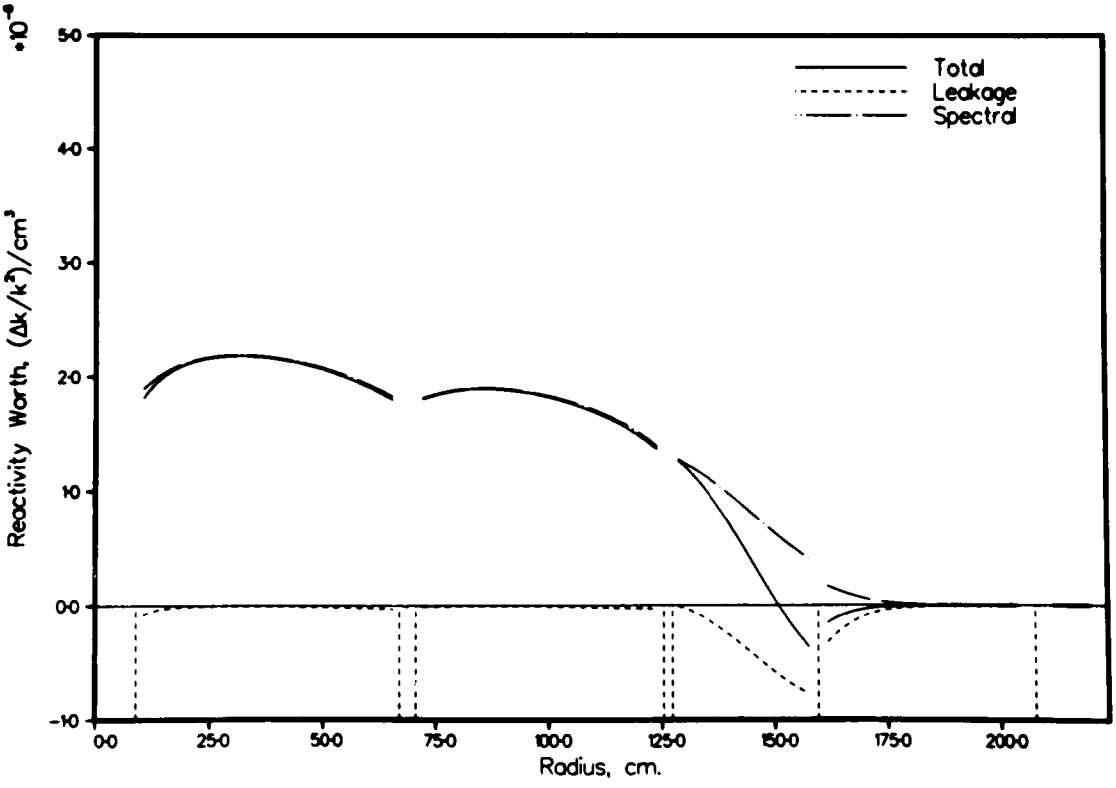

Fig. 10a. Radial Variation of Sodium Void Reactivity in Carbide Reactor at BOL (at Mid-Plane)

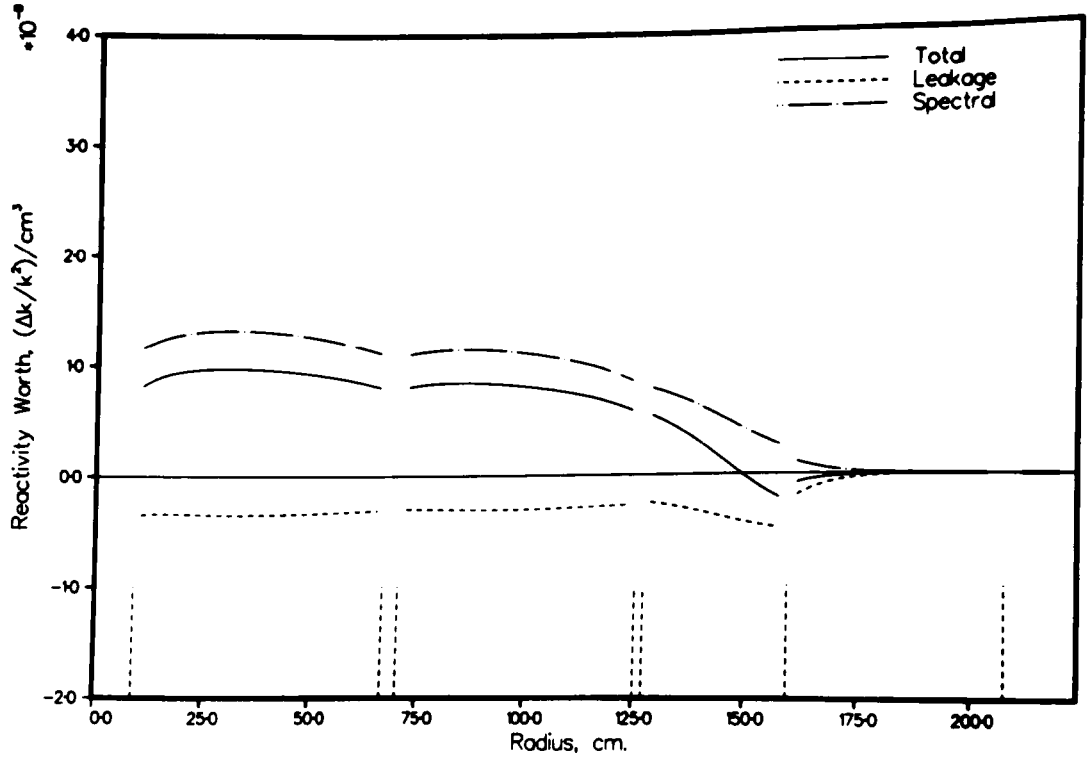

Fig. 10b. Radial Variation of Sodium Void Reactivity in Carbide Reactor at BOL (at 30 cm from Mid-Plane)

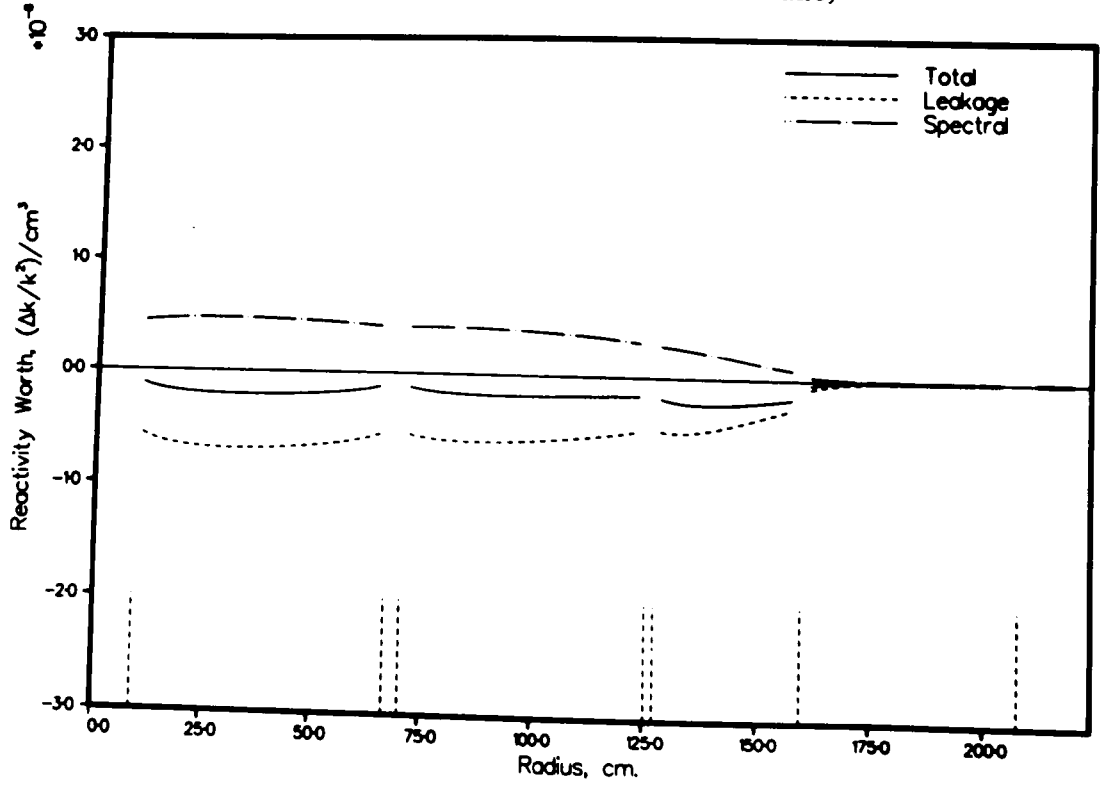

Fig. 10c. Radial Variation of Sodium Void Reactivity in Carbide Reactor at BOL (at 49 cm from Mid-Plane)

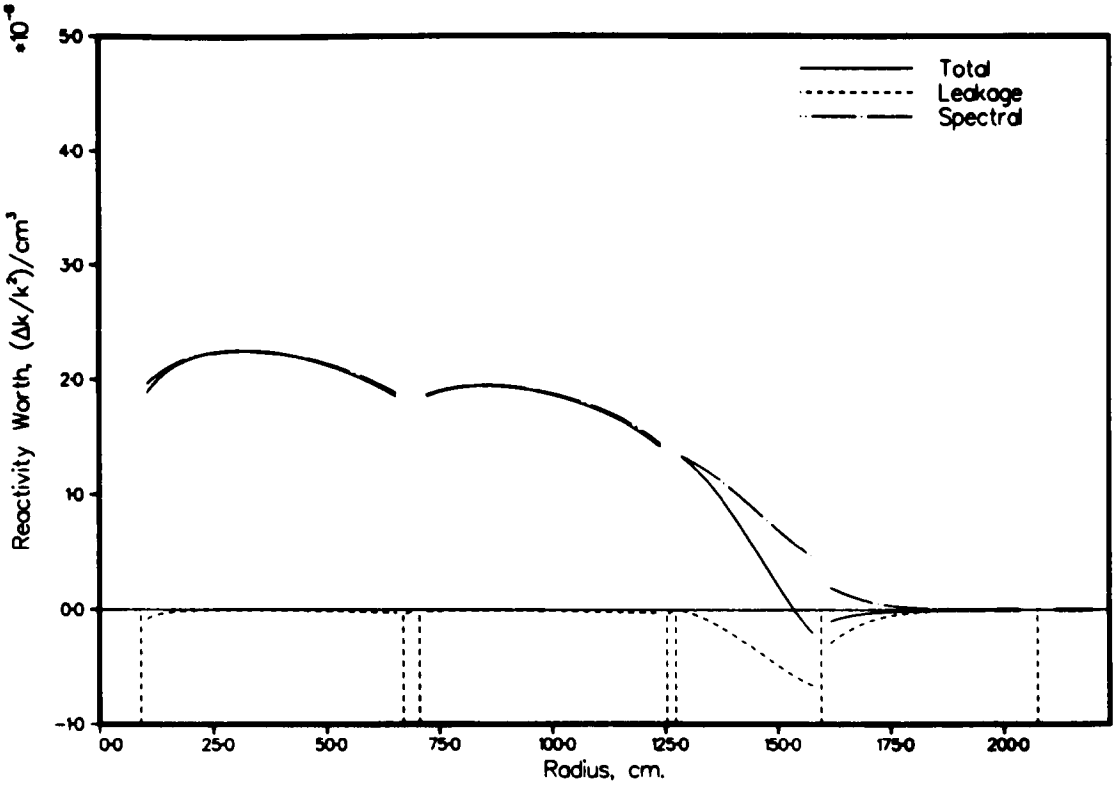

Fig. 11a. Radial Variation of Sodium Void Reactivity in Carbide Reactor at BOEC (at Mid-Plane)

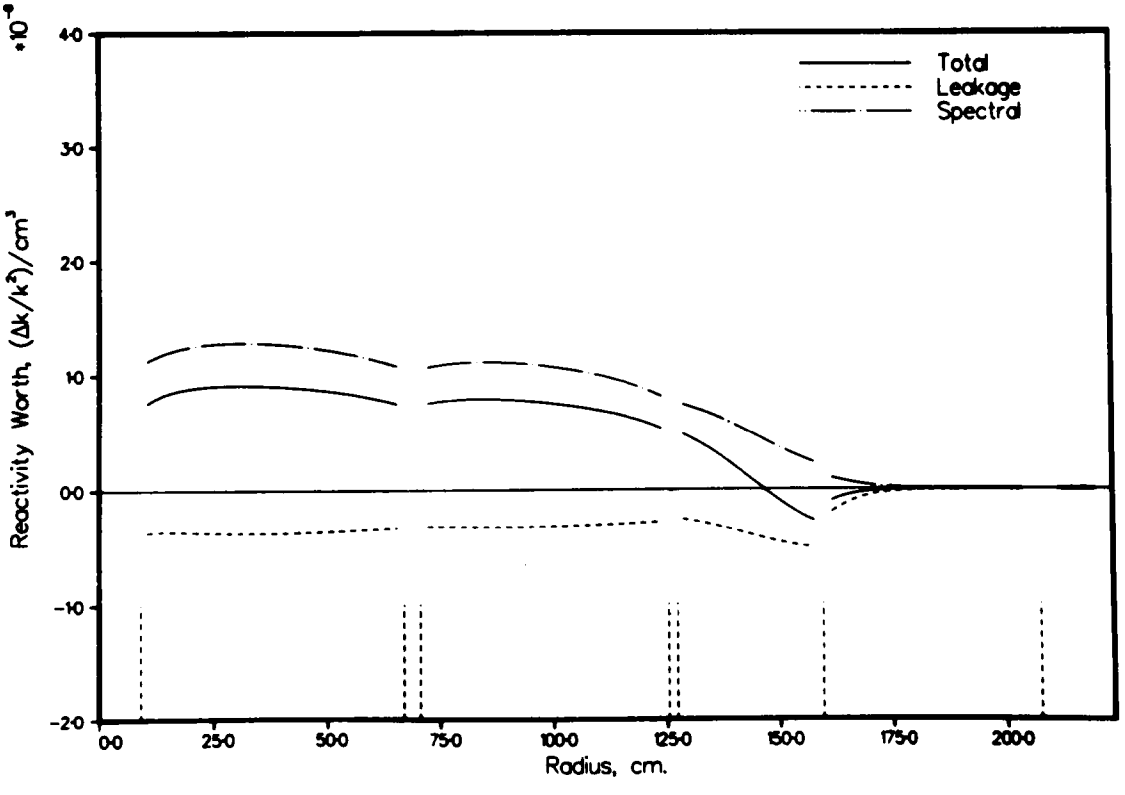

Fig. 11b. Radial Variation of Sodium Void Reactivity in Carbide Reactor at BOEC (at 30 cm from Mid-Plane)

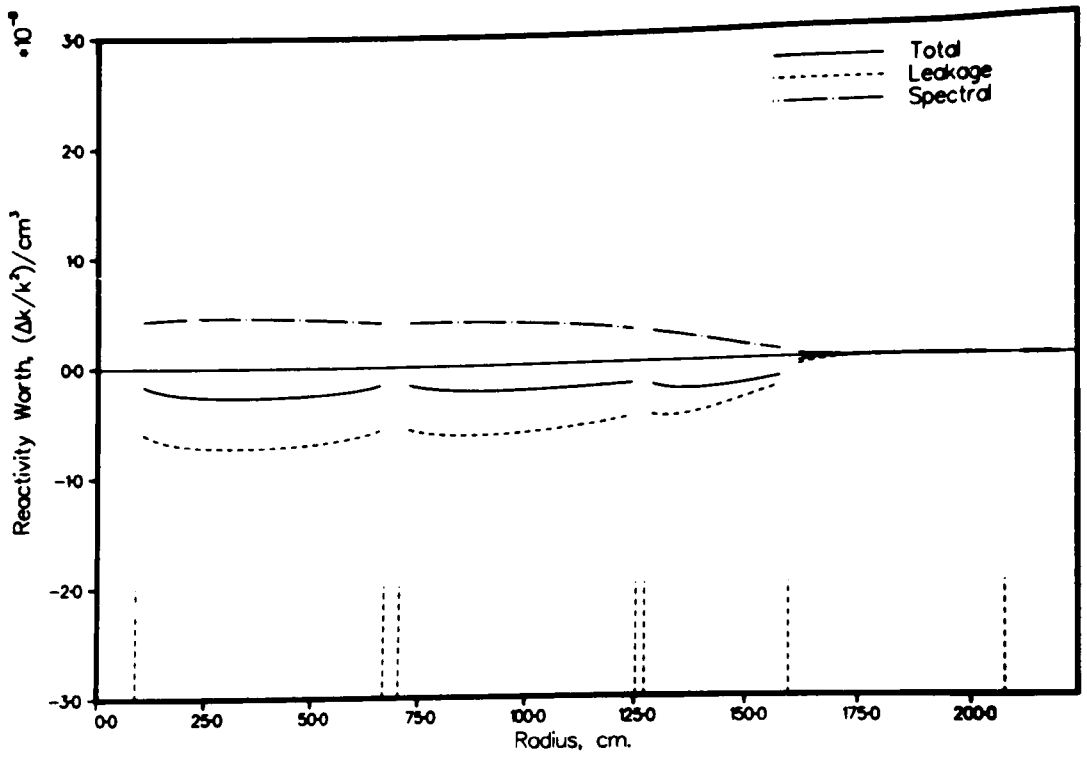

Fig. 11c. Radial Variation of Sodium Void Reactivity in Carbide Reactor at BOEC (at 49 cm from Mid-Plane)

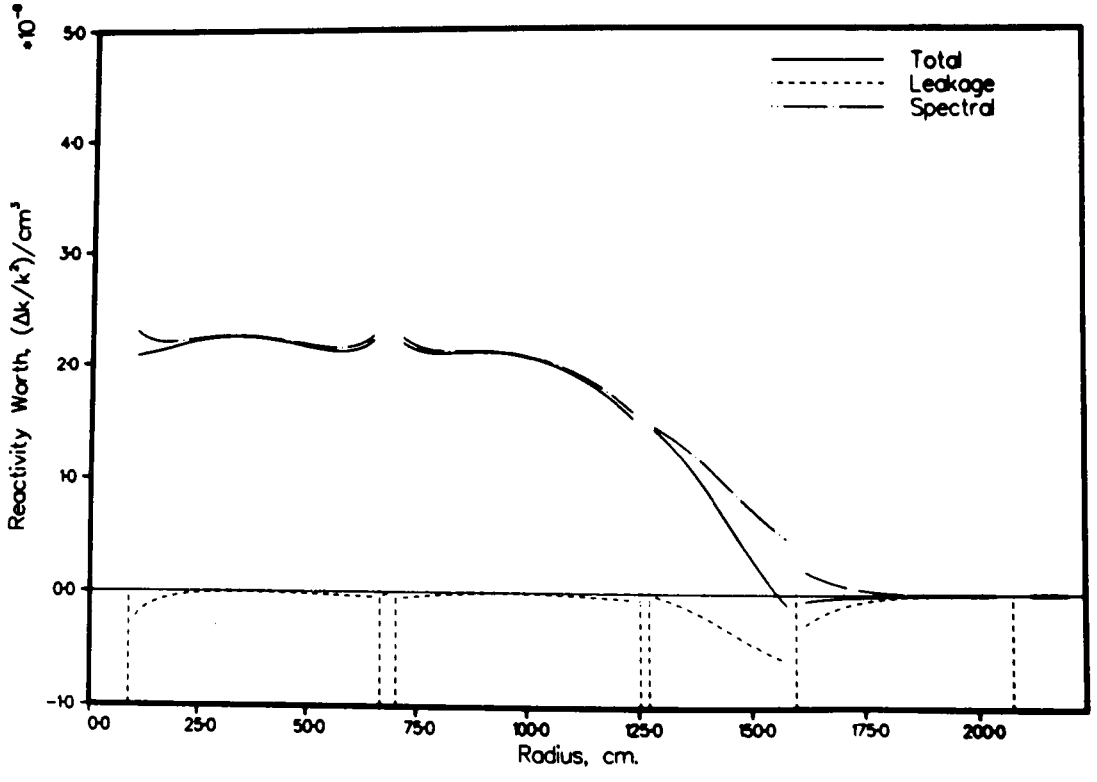

Fig. 12a. Radial Variation of Sodium Void Reactivity in Carbide Reactor at EOEC (at Mid-Plane)

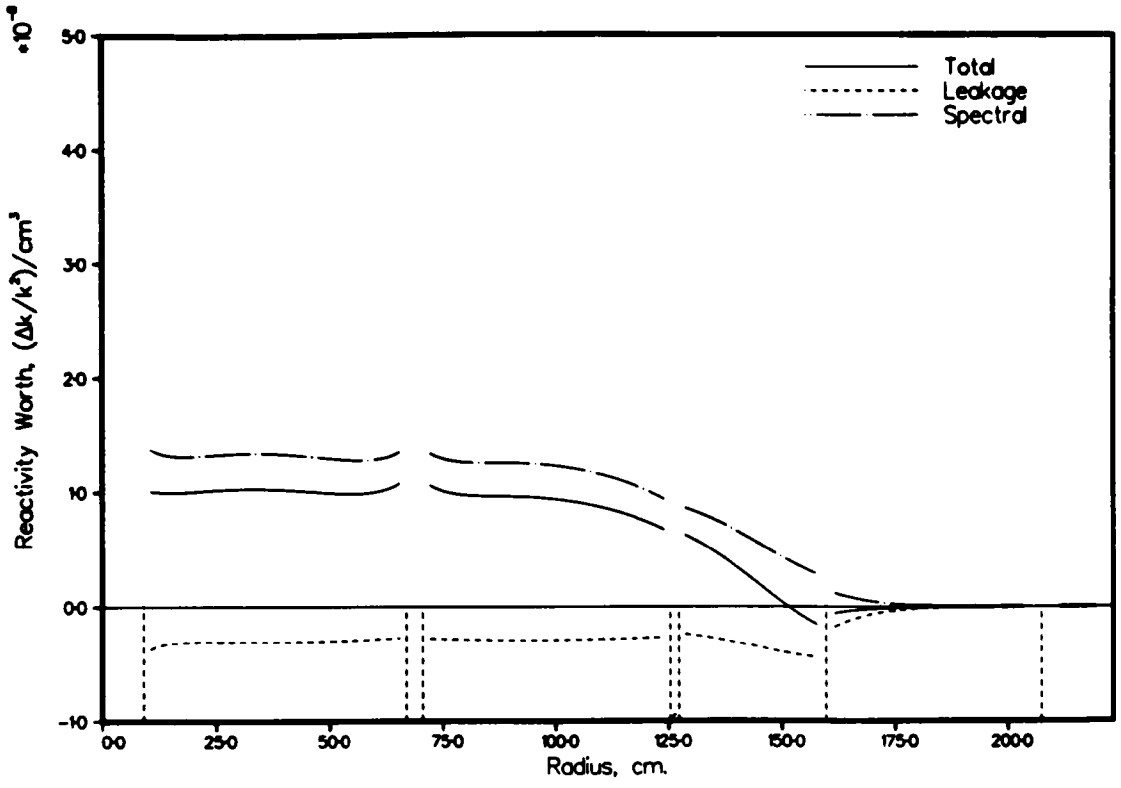

Fig. 12b. Radial Variation of Sodium Void Reactivity in Carbide Reactor at EOEC (at 30 cm from Mid-Plane)

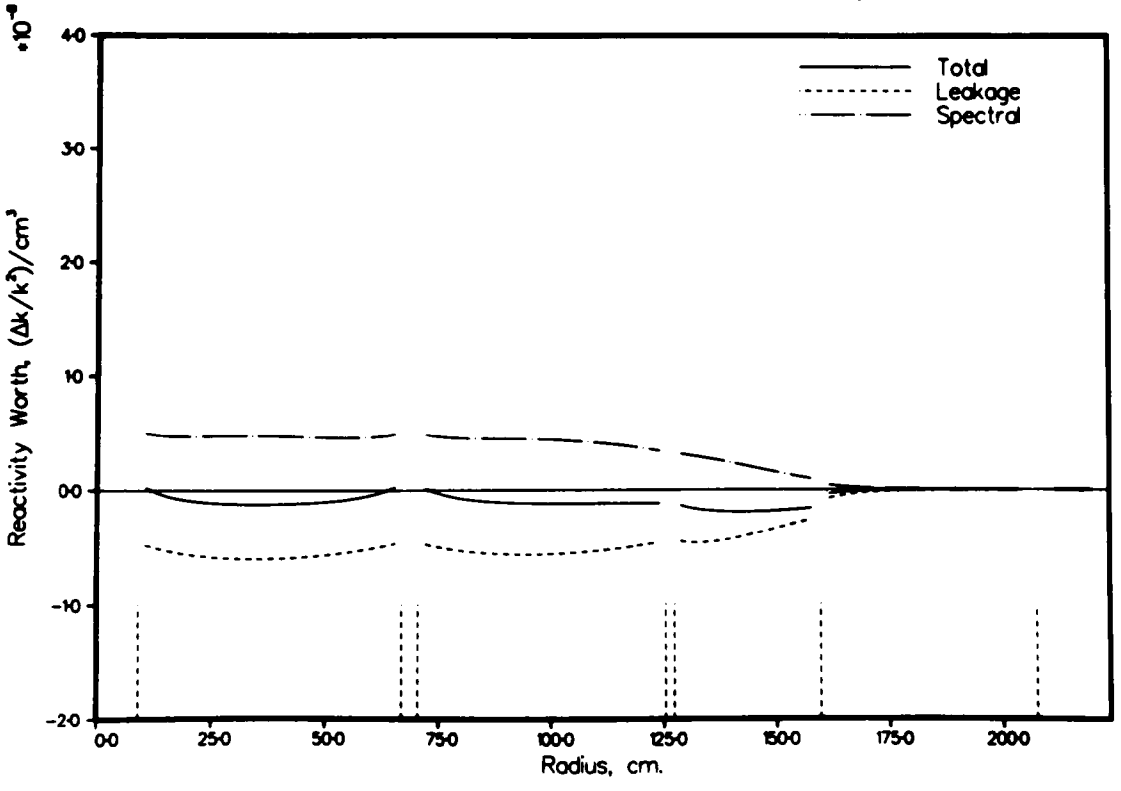

Fig. 12c. Radial Variation of Sodium Void Reactivity in Carbide Reactor at EOEC (at 49 cm from Mid-Plane)

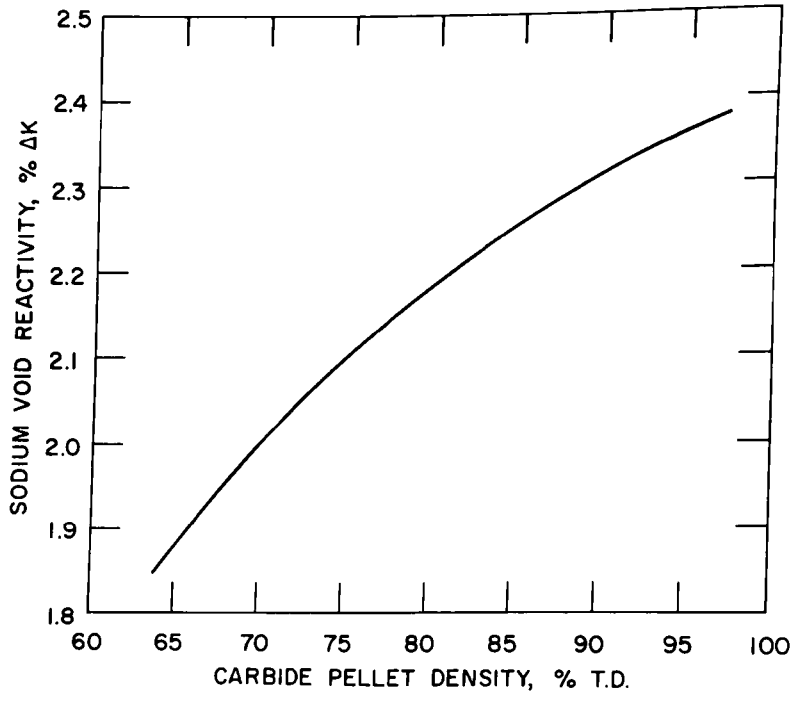

Fig. 13. Dependence of Sodium Void Reactivity on Fuel Density

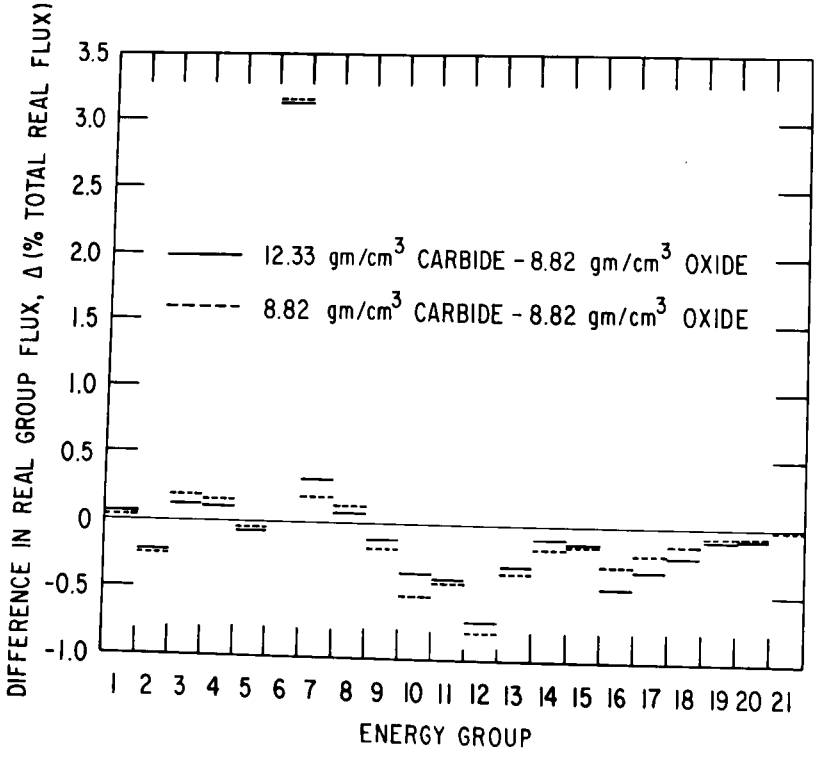

Fig. 14. Comparison of Real Spectra

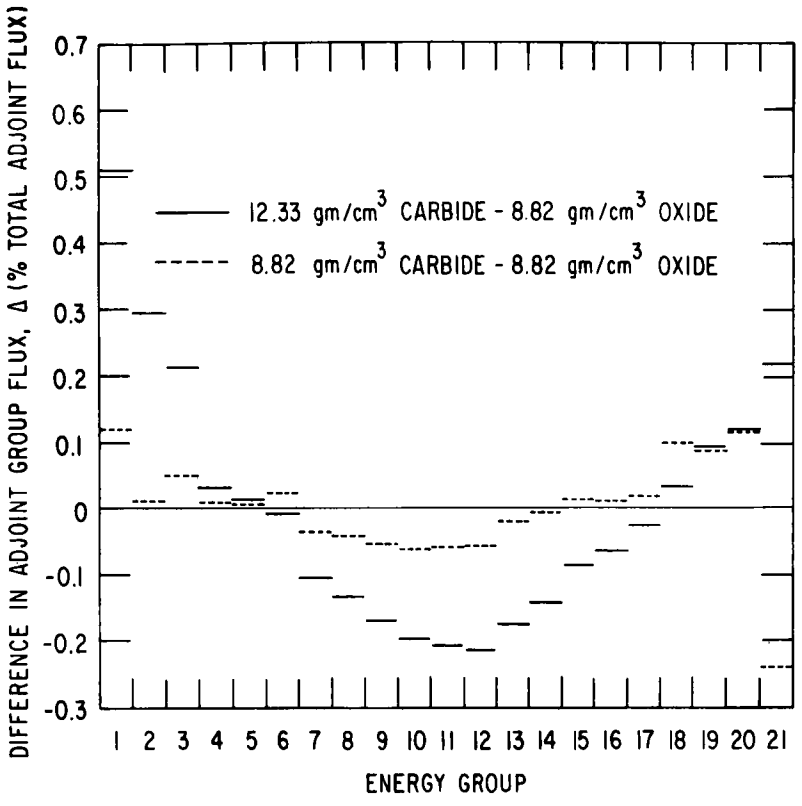

Fig. 15. Comparison of Adjoint Spectra

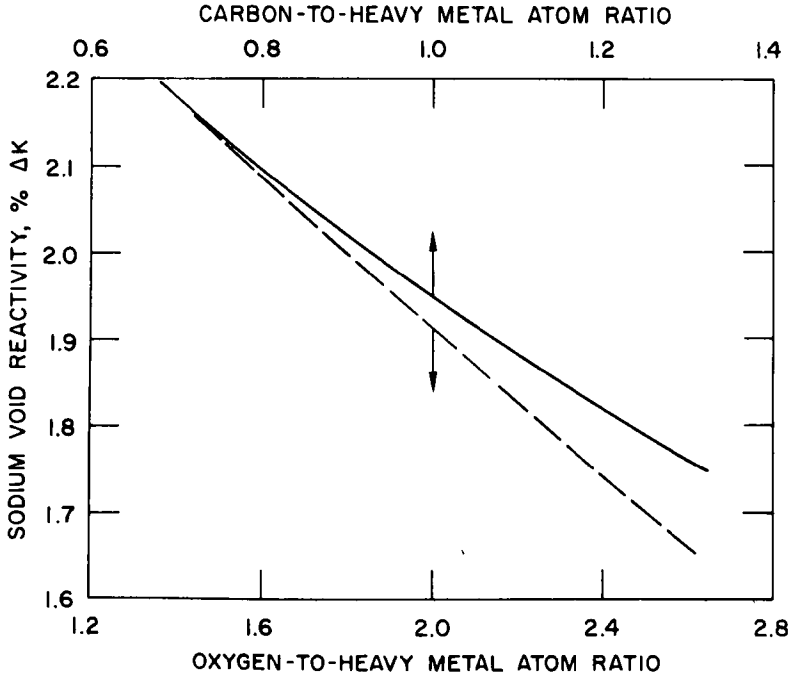

Fig. 16. Dependent of Sodium Void Reactivity on Oxygen- or Carbon-to-Heavy Metal Ratio

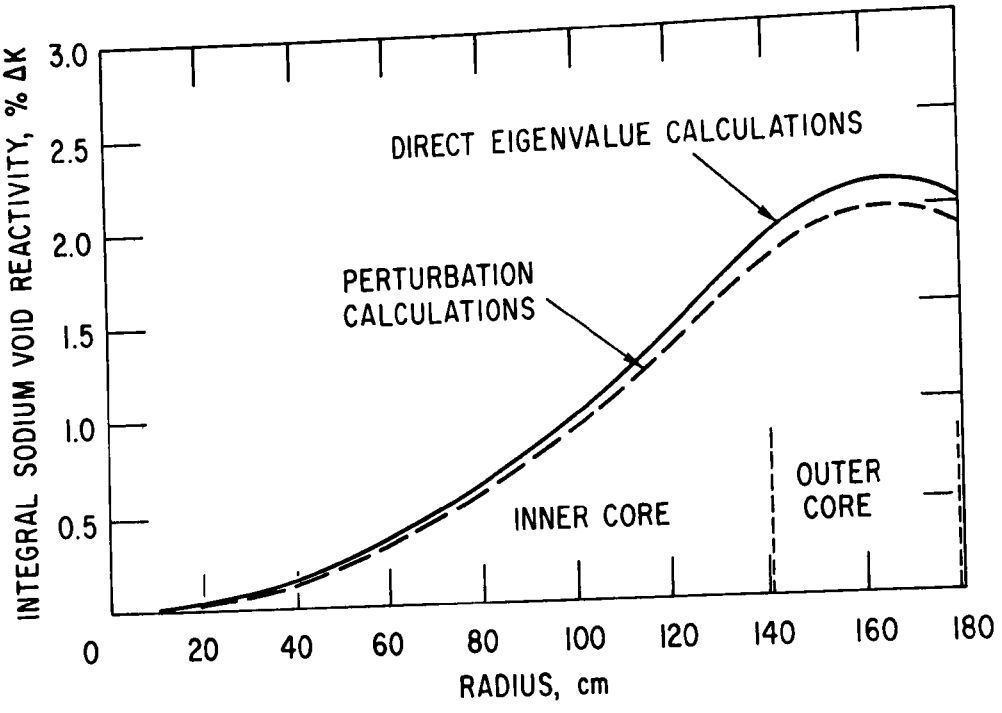

Fig. 17. Integral Sodium Void Reactivity of Oxide Reactor

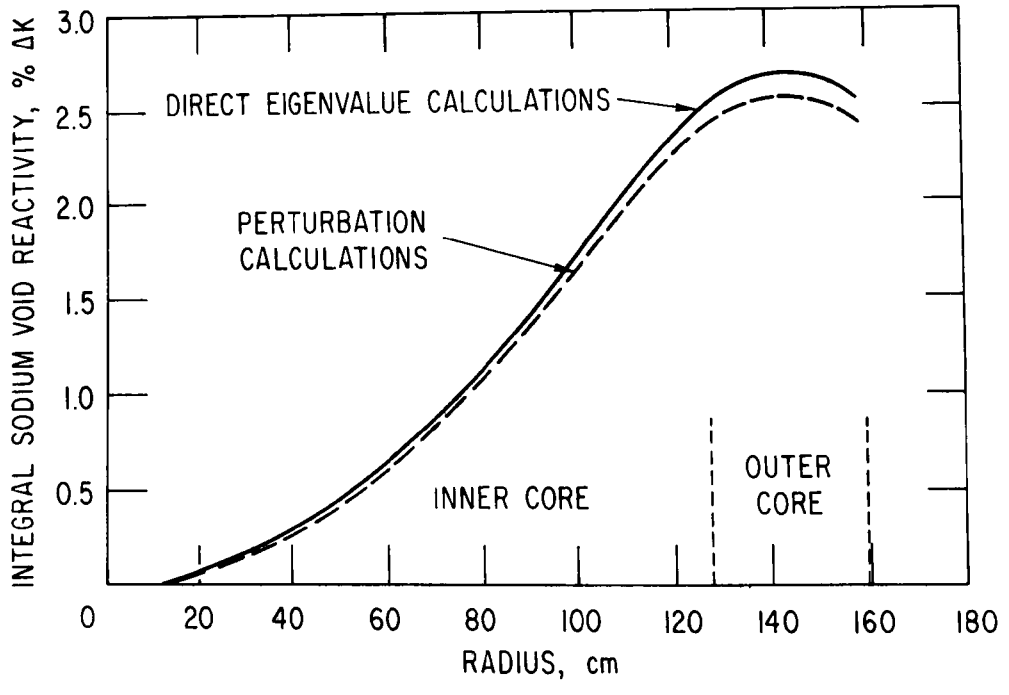

Fig. 18. Integral Sodium Void Reactivity of Carbide Reactor

TABLE I. 3000 MWth Oxide Reactor Design Descriptions

Fuel Assembly Design		
Lattice pitch, in.		6.548
Duct outside width across flats, in.		6.238
Duct inside width across slats, in.		5.968
Duct wall thickness, in.		0.135
Duct wall composition		SS-316
Maximum stress in duct wall, psi		15,800
Sodium gap between assemblies, in.		0.310
Unit cell area, sq. in.		37.1287
Number of fuel pins per assembly		271
Spacer concept		Wire Wrap
Pitch (triangular), in.		0.3624
Fuel pin diameter, in.		0.300
Fuel pin pitch/diameter		1.208
Length of fuel bundle, in.		112.0
Active core height, in.		40.0
Axial blanket thickness, in.		13.0
Axial reflector thickness, in.		3.0
Plenum length, in.		40.0
Plenum position		Bottom
Volume Fractions at Beginning of Life		
Fuel at 91.4% T.D. (pellet)		0.3845
Coolant	0.2926	
Interassembly Gap	0.0924	
Total Sodium		0.3848
Clad	0.1164	
Spacer	0.0224	
Duct	0.0769	
Total Structural		0.2157
Pellet-Clad Gap		0.0150
Sum		1.0000
Total Heavy Metal in Core, kg		35,652.
Weight of Pin Bundle, kg		
Fuel		154,463
Clad	62.985	
Spacer	10,860	
Duct (112.0 in. section)	41.175	
Total Structural		115.019
Axial Reflector		11.582
Total		281.065

TABLE I. (continued)

General Plant Data	
Power, MWt	3116
Core arrangement	Hexagonal
Number of rows in inner core	10
Number of rows in outer core	3
Number of core lattice positions	402
Number of driver assemblies	383
Number of Control rod positions	19
Thermal Hydraulic Data	
Core inlet temperature, ^{o}F	720
Average temperature rise across core, ^{o}F	280
Average driver fuel outlet temperature, ^{o}F	1,000
Maximum coolant velocity, ft/sec	28
Total reactor coolant flow, lb/hr	1.477×10^{8}
Pressure drop across pin bundle, psi.	67
Fuel Pin Data	
Fuel pellet density, % T.D.	91.4
Diametric gap, mils.	5.0
Fuel pin bond	Helium
Smeared fuel density, planar nominal, % T.D.	88.0
Fuel pin outer diameter, in.	0.300
Fuel cladding thickness, mils.	18.0
Fuel cladding composition	SS-316
Peak linear power in fuel, kw/ft	13.5
Average linear power in fuel, kw/ft	8.2
Fuel Cycle Data	
Charge Pu grade	LWR Discharge
Fuel cycle length, yr.	1
Full power days per year	300
Core fuel residence time, yrs.	2

TABLE II. Reactor Conditions at Beginning of Life and Beginning and End of Equilibrium Cycle for 3000 MWth Oxide Reactor

	BOL	BOC	EOC
Charge Fuel Enrichment, % Pu			
Inner Core	14.13	14.37	--
Outer Core	17.63	17.98	-
Outer/Inner Core	1.248	1.251	-
Core Peak/Average Power[a]	1.464	1.432	1.409
Conversion Ratio			
Inner Core	0.98	0.96	0.96
Outer Core	0.75	0.75	0.79
Axial Blanket	--	20.03	7.08
Radial Blanket	--	9.40	6.46
Instantaneous Breeding Ratio	1.29	1.26	1.25
Compound System Doubling Time, yrs.	--	--	25.6
Fissile Loading, kg			
Inner Core	2,198	2,219	2,184
Outer Core	1,854	1,844	1,757
Axial Blanket	--	101	290
Radial Blanket	--	352	519
Total	4,052	4,516	4,750
Heavy Metal Loading, kg			
Inner Core	19,809	--	-
Outer Core	13,392	--	-
Axial Blanket	22,132	--	-
Radial Blanket	52,453	--	-
Total	107,786	--	-
Specific Inventory, kg fissile/MWe	3.26	3.63	3.82
Specific Power, MWt/kg fissile	0.769	0.690	0.656
Maximum Fluence, 10^{23} nvt (E>1.0 MEV)	--	--	1.81
Average Burnup, 10^3 MWD/MT			
Inner Core	--	13.92	41.44
Outer Core	--	11.55	34.10
Axial Blanket	--	0.46	1.66
Radial Blanket	--	0.89	1.45
Max. Pellet Discharge Burnup, 10^3 MWD/MT	--	--	71.3
Burnup Swing, Δk_{eff} (Equilibrium Cycle)	--	--	-0.0221

[a] as calculated

TABLE III. 3000 MWth Carbide Reactor Design Descriptions

Fuel Assembly Design		
Lattice Pitch, in.		6.7662
Duct outside width across flats, in.		6.473
Duct inside width across flats, in.		6.233
Duct wall thickness, in.		0.120
Duct wall composition		SS-316
Maximum stress in duct wall, psi.		10,870.
Sodium gap between assemblies, in.		0.293
Unit cell area, sq. in.		39.6483
Number of fuel pins per assembly		169.
Spacer concept		GRIDS
Pitch (triangular), in.		0.474
Fuel pin diameter, in.		0.375
Fuel pin pitch/diameter		1.263
Length of fuel bundle, in.		112.0
Active core height, in.		40.0
Axial blanket thickness, in.		13.0
Axial reflector thickness, in.		3.0
Plenum length, in.		40.0
Plenum position		TOP
Volume Fractions at Beginning of Life		
Fuel at 95.0% T.D. (Pellet)		0.3757
Coolant	0.3741	
Sodium bond	0.0228	
Interassembly gap	0.0847	
Total sodium		0.4816
Clad	0.0723	
Spacer	0.0038	
Duct	0.0666	
Total structural		0.1427
Sum		1.0000
Weight of Pin Bundle, KG		
Fuel		208.608
Clad	41.785	
Spacer	2.173	
Duct (112.0 inch section)	39.625	
Total structural		83.583
Axial reflector		12.335
Total		304.526

TABLE III. (continued)

General Plant Data	
Power, MWt	3,145
Core arrangement	HEXAGONAL
Number of rows in inner core	9
Number of rows in outer core	2
Number of core lattice positions	313
Number of driver assemblies	294
Number of control rod positions	19
Thermal Hydraulic Data	
Core inlet temperature, deg. F	720.
Average temperature rise across core, deg. F	280.
Average driver fuel outlet temperature, deg. F	1,000.
Maximum coolant velocity, ft/sec	28.
Total reactor coolant flow, lb/hr	1.266×10^8
Pressure drop across pin bundle, psi.	34.
Fuel Pin Data	
Fuel pellet density, % T.D.	95.0
Diametric gap, mils.	10.0
Fuel pin bond	SODIUM
Smeared fuel density, planar nominal, % T.D.	89.6
Fuel pin outer diameter, in.	0.375
Fuel cladding thickness, mils.	15.0
Fuel cladding composition	SS-316
Peak linear power in fuel, kw/ft	30.0
Average linear power in fuel, kw/ft	18.2
Fuel Cycle Data	
Charge Pu grade	LWR DISCHARGE
Fuel cycle length, yr.	1
Full power days per year	300
Core fuel residence time, yrs.	2
Blanket fuel residence time, yrs.	5

TABLE IV. Reactor Conditions at Beginning of Life and Beginning and End of Equilibrium Cycle for 3000 MWth Carbide Reactor

	BOL	BOC	EOC
Charge Fuel Enrichment, % Pu			
Inner Core	10.91	10.68	-
Outer Core	14.52	14.47	-
Outer/Inner Core	1.330	1.355	-
Core Peak/Average Power[a]	1.478	1.445	1.426
Conversion Ratio			
Inner Core	1.26	1.23	1.13
Outer Core	0.90	0.91	0.92
Axial Blanket	-	20.28	7.13
Radial Blanket	-	9.22	6.44
Instantaneous Breeding Ratio	1.62	1.57	1.47
Compound System Doubling Time, yrs.	-	9.7	
Fissile Loading, kg			
Inner Core	1,910	1,928	2,029
Outer Core	1,557	1,535	1,502
Axial Blanket	-	106	308
Radial Blanket	-	430	626
Total	3,467	3,999	4,465
Heavy Metal Loading, kg			
Inner Core	22,397	-	-
Outer Core	13,727	-	-
Axial Blanket	23,480	-	-
Radial Blanket	68,246	-	-
Total	127,850	-	-
Specific Inventory, kg fissile/MWe	2.76	3.18	3.55
Specific Power, MWt/kg fissile	0.907	0.786	0.704
Maximum Fluence, 10^{23} MWD/MT (E > 0.1 MeV)	-	-	2.00
Average Burnup, 10^3 MWD/MT			
Inner Core	-	12.3	37.1
Outer Core	-	10.6	31.6
Axial Blanket	-	0.5	1.8
Radial Blanket	-	0.9	1.5
Max. Pellet Discharge Burnup, 10^3 MWD/MT	-	-	67.0
Burnup Swing, Δk_{eff} (Equilibrium Cycle)	-	-	+0.0128

[a] as calculated

TABLE V. Sodium Void Reactivity of 3000 MWth Oxide Reactor (Direct Eigenvalue Calculations)

Region(s) Voided	$\Delta k_{eff}/k_{eff}$ BOL	BOEC	EOEC
Inner Core[a]	0.0177 (0.0135)	0.0190 (0.0144)	0.0220 (0.0167)
Outer Core[a]	0.0024 (0.0018)	0.0034 (0.0026)	0.0032 (0.0024)
Total Core[a]	0.0203 (0.0154)	0.0226 (0.0172)	0.0256 (0.0195)
Control Rod Channels	0.0001	0.0004	-0.0018
Entire Reactor[b]	0.0179	0.0204	0.0210
Core Max. Void Reactivity[a]	0.0212	0.0236	0.0267

[a]Excluding control rod channels; data in parenthesis exclude voiding of gaps between assemblies

[b]Including control rod channels

TABLE VI. Sodium Void Reactivities in Core of Oxide Reactor[a] (Perturbation Calculations)

	$\Delta k/k$ BOL	BOEC	EOEC
Leakage	-0.0101 (-0.0098)	-0.0095 (-0.0092)	-0.0087 (-0.0084)
Spectral	+0.0287 (+0.0246)	+0.0302 (+0.0261)	+0.0321 (+0.0279)
Net	+0.0186 (+0.0148)	+0.0207 (+0.0169)	+0.0234 (+0.0195)

[a]Control rod channels not voided; values in parentheses exclude the effects of microscopic cross-section changes due to spectral hardening

TABLE VII. Sodium Void Reactivity of 3000 MWth Carbide Reactor (Direct Eigenvalue Calculations)

Region(s) Voided	$\Delta k_{eff}/k_{eff}$ BOL	BOEC	EOEC
Inner Core[a]	0.0239 (0.0197)	0.0257 (0.0212)	0.0301 (0.0248)
Outer Core[a]	0.0012 (0.0010)	0.0025 (0.0021)	0.0035 (0.0029)
Total Core[a]	0.0255 (0.0210)	0.0285 (0.0235)	0.0334 (0.0275)
Control Rod Channels	-0.0015	-0.0012	0.0011
Entire Reactor[b]	0.0221	0.0253	0.0322
Core Max. Void Reactivity[a]	0.0267	0.0299	0.0350

[a]Excluding control rod channels; data in parenthesis exclude voiding of gaps between assemblies

[b]Including control rod channels

TABLE VIII. Sodium Void Reactivities in Core of Carbide Reactor[a] (Perturbation Calculations)

	$\Delta k/k$ BOL	BOEC	EOEC
Leakage	-0.0124 (-0.0122)	-0.0115 (-0.0113)	-0.0110 (-0.0108)
Spectral	+0.0370 (+0.0318)	+0.0386 (+0.0334)	+0.0423 (+0.0371)
Net	+0.0246 (+0.0196)	+0.0271 (+0.0221)	+0.0313 (+0.0263)

[a]Control rod channels not voided; values in parentheses exclude the effects of microscopic cross section changes due to spectral hardening.

TABLE IX. Comparisons of Spectral Effects of Sodium Voiding

	Oxide			Carbide		
	BOL	BOEC	EOEC	BOL	BOEC	EOEC
Median energy of flux in core, 100 keV						
Core with sodium	1.330	1.338	1.313	1.538	1.548	1.596
Core without sodium	1.518	1.527	1.505	1.843	1.855	1.907
Difference	0.188	0.189	0.192	0.305	0.307	0.311
Fission neutron per absorption in heavy metal in core						
Core with sodium	1.341	1.352	1.339	1.264	1.272	1.310
Core without sodium	1.399	1.411	1.402	1.338	1.347	1.387
Difference	0.058	0.059	0.063	0.074	0.075	0.077
Heavy metal/total absorption in core						
Core with sodium	0.9354	0.9243	0.9006	0.9641	0.9531	0.9324
Core without sodium	0.9427	0.9327	0.9114	0.9703	0.9606	0.9419
Difference	0.0073	0.0084	0.0108	0.0062	0.0075	0.0095
Fission neutrons per absorption in core						
Core with sodium	1.254	1.250	1.206	1.218	1.212	1.221
Core without sodium	1.319	1.316	1.278	1.298	1.294	1.306
Difference	0.065	0.066	0.072	0.080	0.082	0.085

TABLE X. Dependence of Sodium Void Reactivity on Fuel Density (Using carbide pellets in oxide design; BOL conditions; direct eigenvalue calculations)

Case	1	2	3	4
Fuel Pellet Density, % T.D.	95	85	75	68
Heavy Metal Density, gm/cm^3	12.33	11.03	9.73	8.82
Core Fertile/Fissile Mass	9.55	8.91	8.09	7.42 (7.19)[a]
Burnup Swing, Δk	0.0133	0.0033	-0.0088	-0.0189
$k_{eff}^{(BOL)}$	1.0000	1.0000	1.0088	1.0189
Sodium Void Reactivity, $\Delta k/k$	0.0236	0.0225	0.0210	0.0195 (0.0191)[a]
Core Median Energy, 10^5 eV	1.509	1.515	1.527	1.539
Core Leakage/Fission Neutron				
with sodium	0.1604	0.1764	0.1923	0.2037
without sodium	0.1755	0.1940	0.2128	0.2266
Difference	0.0151	0.0176	0.0205	0.0229
Reactor η				
with sodium	1.0156	1.0190	1.0305	1.0427
without sodium	1.0428	1.0457	1.0567	1.0682
Difference	0.0272	0.0267	0.0262	0.0255

[a]For oxide fuel with 8.82 gm/cm^3 heavy metal (91.4% T.D.)

TABLE XI. Dependence of Sodium Void Reactivity on Oxygen-to-Heavy Metal Ratio
(8.82 gm/cm^3 heavy metal density; BOL conditions; direct eigenvalue calculations)

Oxygen / Heavy Metal	1.6	2.0	2.4
Sodium Void Reactivity, $\Delta k/k$	0.0209	0.0191	0.0174
Core Median Flux Energy, 10^5 eV	1.370	1.300	1.239
Core Leakage/Fission Neutron			
with sodium	0.1848	0.1747	0.1653
without sodium	0.2046	0.1931	0.1825
Difference	0.0198	0.0184	0.0172
Reactor η			
with sodium	1.0434	1.0453	1.0485
without sodium	1.0705	1.0699	1.0710
Difference	0.0271	0.0246	0.0225

TABLE XII. Dependence of Sodium Void Reactivity on Carbon-to-Heavy Metal Ratio
(8.82 gm/cm^3 heavy metal density; BOL conditions; direct eigenvalue conditions)

Carbon / Heavy Metal	0.8	1.0	1.2
Sodium Void Reactivity, $\Delta k/k$	0.0209	0.0195	0.0182
Core Median Flux Energy, 10^5 eV	1.587	1.539	1.494
Core Leakage/Fission Neutron			
with sodium	0.2127	0.2037	0.1954
without sodium	0.2368	0.2266	0.2172
Difference	0.0241	0.0229	0.0218
Reactor η			
with sodium	1.0370	1.0427	1.0483
without sodium	1.0643	1.0682	1.0722
Difference	0.0273	0.0255	0.0239

TABLE XIII. Doppler Coefficients for Entire Oxide Reactor[a] (650 → 2200°k)

	$-T\frac{dK}{dT} * 10^4$		
	BOL	BOEC	EOEC
Core with sodium	109.5	103.5	105.7
Core without sodium	79.2	74.4	76.9

[a]Direct Eigenvalue Calculations

TABLE XIV. Doppler Coefficients by Reactor Region for 3000 MWth Oxide Reactor (1300 to 2200°K, core with sodium)[a]

	$-T\frac{dk}{dT} \times 10^4$		
Reactor Region	BOL	BOEC	EOEC
Inner Core	72.6	65.2	66.3
Outer Core	22.2	21.4	19.5
Total Core	94.8	86.6	85.8
Axial Blanket	6.4	7.2	10.4
Radial Blanket	3.1	4.6	4.4
Total Core and Blankets	104.3	98.4	100.6

[a]Direct Eigenvalue Calculations

TABLE XV. Doppler Coefficients by Reactor Region for 3000 MWth Oxide Reactor (1300 to 2200°k,,core without sodium) [a]

Reactor Region	$-T\frac{dk}{dT} \times 10^4$ BOL	BOEC	EOEC
Inner Core	50.1	44.1	44.7
Outer Core	14.8	14.2	13.1
Total Core	64.9	58.3	57.8
Axial Blanket	6.2	6.9	9.9
Radial Blanket	2.7	4.0	3.9
Total Core and Blankets	73.8	69.2	71.6

[a] Direct Eigenvalue Calculations

TABLE XVI. Doppler Coefficients of Oxide Reactor: Direct Eigenvalue Calculations vs. Perturbation Calculations

(1300 → 2200°K, BOL)

Reactor Region	$-T\frac{dK}{dT} \times 10^4$ Core With Sodium (a)	(b)	Core Without Sodium (a)	(b)
Inner core	72.6	76.2	50.1	52.0
Outer core	22.2	22.5	14.8	15.1
Total core	94.8	98.7	64.9	67.1
Axial blanket	6.4	7.0	6.2	6.8
Radial blanket	3.1	3.4	2.7	3.0
Total core and blankets	104.3	109.1	73.8	76.9

(a) Direct eigenvalue calculations

(b) Perturbation calculations

TABLE XVII. Doppler Coefficients for Entire Carbide Reactor[a]

(650 → 2200°K)

	$-T\frac{dK}{dT} * 10^4$		
	BOL	BOEC	EOEC
Core with sodium	110.0	104.2	85.8
Core without sodium	71.9	69.6	59.4

[a]Direct Eigenvalue Calculations

TABLE XVIII. Doppler Coefficients by Reactor Region for 3000 MWth Carbide Reactor [a]

(1100 to 2200 °k, core with sodium)

	$-T\frac{dk}{dT} * 10^4$		
Reactor Region	BOL	BOC	EOC
Inner core	78.9	71.8	55.8
Outer Core	19.9	19.4	17.2
Total Core	98.8	91.2	73.0
Axial blanket	5.2	5.9	6.2
Radial blanket	2.5	3.7	4.0
Total core and blankets	106.5	100.8	83.2

[a]Direct Eigenvalue Calculations

TABLE XIX. Doppler Coefficients by Reactor Region for 3000 MWth Carbide Reactor [a]

(1100 to 2200 ^{o}k, core without sodium)

Reactor Region	$-T \frac{dk}{dT} * 10^4$		
	BOL	BOC	EOC
Inner core	48.4	44.5	36.0
Outer core	11.6	11.5	10.0
Total core	60.0	56.0	46.0
Axial blanket	5.9	6.7	6.9
Radial blanket	2.5	3.6	3.8
Total core and blanket	68.4	66.3	56.7

[a]Direct Eigenvalue Calculations

TABLE XX. Dependences of Doppler Coefficient on Fuel Type and Heavy Metal Density

	Reactor Model			
	Oxide[(a)]	Carbide[(b)]	Hypothetical Carbide[(c)]	Hypothetical Carbide[(d)]
Heavy Metal Density, gm/cm^3	8.82	12.33	12.33	8.82
Fertile-to-Fissile Ratio	7.19	9.42	9.55	7.42
Core Median Flux Energy, 10^5 eV	1.33	1.54	1.51	1.57
Doppler Coefficient, 10^{-4} °K^{-1}	-94.8	-98.8	-98.6	-83.8

(a)Described in Section III.A

(b)Described in Section III.B

(c)Using carbide pellet (95% T.D.) in oxide design

(d)Using carbide pellet (68% T.D.) in oxide design

Distribution for ANL-78-41

Internal:

J. A. Kyger
R. Avery
L. Burris
D. W. Cissel
S. A. Davis
B. R. T. Frost
D. C. Rardin
R. J. Teunis
C. E. Till
R. S. Zeno
G. H. Golden
H. O. Monson
J. H. Kittel
P. B. Abramson
P. I. Amundson
W. P. Barthold
J. C. Beitel
C. Bowers
S. G. Carpenter
Y. I. Chang
D. R. Ferguson
H. Henryson
H. H. Hummel
R. N. Hwang
P. S. K. Lam
L. G. LeSage
M. J. Lineberry
H. F. McFarlane
R. D. McKnight
Y. Orechwa
S. F. Su (15)
B. J. Toppel
A. Travelli
R. B. Turski
D. C. Wade
A. B. Krisciunas
ANL Contract File
ANL Libraries (5)
TIS Files (6)

External:

DOE-TIC, for distribution per UC-79d (264)
Manager, Chicago Operations Office
Chief, Chicago Patent Group
Director, Reactor Programs Div., CH
Director, CH-INEL
Director, DOE-RRT (2)
President, Argonne Universities Association
Applied Physics Division Review Committee:
P. W. Dickson, Jr., Westinghouse Electric Corp.
R. L. Hellens, Combustion Engineering, Inc.
W. B. Loewenstein, Electric Power Research Inst.
R. F. Redmond, Ohio State U.
R. Sher, Stanford U.
D. B. Wehmeyer, Detroit Edison Co.
S. A. Werner, U. Missouri

☆ U.S. GOVERNMENT PRINTING OFFICE: 1977 750-133/31